

Universidade de Lisboa

Faculdade de Ciências

Departamento de Física



Tailoring crimp patterns on electrospun fibers by using thermal shrinkage

Danielle Ferreira Baptista

Dissertação

Mestrado Integrado em Engenharia Biomédica e Biofísica

Perfil em Engenharia Clínica e Instrumentação Médica

2014

Universidade de Lisboa

Faculdade de Ciências

Departamento de Física



Tailoring crimp patterns on electrospun fibers by using thermal shrinkage

Danielle Ferreira Baptista

Dissertação orientada por : Prof. Hugo Ferreira, Prof. Lorenzo Moroni

2014

"In the middle of every difficulty lies an opportunity."

Albert Einstein

Resumo

A Engenharia de Tecidos apresenta-se como a solução para males como: a incorrecta regeneração natural de tecidos, a diminuta oferta de enxertos e problemas como a rejeição e o desencadeamento de resposta inflamatória a implantes. Como seria possível antever, da teoria à prática decorre uma infinidade de desafios, a utilização de células estaminais provou ser uma boa aposta quando controlada e contida, assim como a utilização de *scaffolds* que incitem a proliferação celular e a regeneração do tecido lesado. A combinação dos dois nem sempre é bem-sucedida, frequentemente surgem problemas como a infiltração celular não homogénea ou inadequabilidade do próprio *scaffold* à aplicação clínica desejada. A estratégia passa por criar *scaffolds* que mimetizem nichos celulares do tecido nativo ou que forneçam pistas às células, e perceber quais as células indicadas ao objectivo e como as controlar *in vitro* e *in vivo*.

A dissertação aqui apresentada discute um novo método que permite criar padrões ondulados em fibras produzidas a partir do electrofiação e deste modo aperfeiçoar os *scaffolds* usados em regeneração de tecidos.

Através do calor, um filme de polímero, onde anteriormente se tinham depositado fibras poliméricas, encolhe levando ao encaracolamento das fibras. Estas abandonam uma conformação linear e assumem um padrão encaracolado. O padrão obtido pode ser modificado e adaptado alterando parâmetros simples, explorados neste trabalho, como a densidade de fibras no filme, tempo de exposição ao calor, orientação com que as fibras são depositadas, tipo de filme utilizado e inclusão ou não de fibras sacrificiais.

No decorrer do projecto os *scaffolds* revelaram-se multifacetados possibilitando uma diversidade estrutural através de simples modificações no processo de fabrico o que se traduz numa mais-valia a nível de possíveis aplicações.

Numa tentativa de solucionar o problema da infiltração celular, muito comum em *scaffolds* produzidos por eletrofiação, estudou-se o encaracolamento das fibras poderia aumentar o espaço vazio dentro da estrutura, incentivando assim a migração celular. Os resultados obtidos mostraram que avaliando os dois tipos *scaffold* é notória a migração celular e uma distribuição mais uniforme e rápida em *scaffolds* enrugados.

Os *scaffolds* enrugados mais densos apresentavam uma topografia semelhante à de tendões e ligamentos. Com base nesta evidência, testou-se a hipótese de que este padrão pudesse induzir e desencadear mecanismos semelhantes aos produzidos quando as células estão na presença de TGF β , factor de crescimento importante no desenvolvimento destas estruturas. Para tal utilizou-se uma linhagem de células transfectadas, MLEC (*mink lung ephiteal cells*), as quais eram sensíveis a presença de TGF β .

Os resultados foram muito promissores e verificou-se que a topografia criada desencadeava mecanismos de sinalização do TGF β podendo ser uma boa aposta para a regeneração destes tecidos.

Em suma, os padrões incluídos em *scaffolds* produzidos por eletrofiação parecem conferir vantagens no que toca a regeneração de tecidos como ligamentos e tendões. Ao assumir-se como um sistema multifacetado e permitindo distribuições celulares mais uniformes, aumenta o leque de possíveis aplicações clínicas. São ainda apresentadas semelhanças morfológicas entre diferentes configurações obtidas com o *scaffold* desenvolvido e tecidos nativos como traqueia, parede arterial, íris e corpo ciliar, que corroboram esta mesma ideia. A proximidade morfológica entre a estrutura desenvolvida e tecidos nativos acresce ainda mais a ideia de que com pequenos ajustes se conseguiria aplicação a diferentes tipos de tecido.

Abstract

Introduction: Tissue engineers aim to regenerate native tissues, since grafting current alternatives such as autologous or allogenic tissues have a finite supply and are characterized by a lot of limitations, among which rejection and disease transmission. The challenge in tissue engineering is to combine cells and materials trying to recreate the appropriate niches for cellular development and later on regenerate human tissues. The difficulties rely on further understanding cell behavior and creating a proper structure that can guide and help cells in the healing process. Several techniques have been employed to produce scaffolds; one of them is electrospinning. This technique is simple, cheap and straightforward but one of the major drawbacks is the lack of cellular infiltration that these scaffolds present. The fiber alignment can be a useful tool to guide cells but it is not enough to induce a proper differentiation. Electrospun scaffolds have the potential to mimic the physico-chemical properties of native extracellular matrix, but need to improve in quality and structural information/cues for cells to follow a specific pathway. Therefore, the aim of this study was to create novel electrospun scaffolds able to surpass current limitations and promote tissue healing.

Materials and Methods: PEOT/PBT fibers were electrospun on poly(lactic acid) (PLA) films and then placed in the oven at a certain temperature and period of time. As a consequence, the film shrunk and the fibers curled assuming a crimp pattern. Several modifications, including different orientations of fiber deposition, the use of sacrificial fibers and different films, were tested in order to create different structural configurations. The scaffolds were seeded with hMSCs (human mesenchymal stem cells) to assess cellular ingrowth and with MLEC (mink lung epithelial cells) to investigate possible similarities between these wavy constructs and native tendon/ligament.

Results: Through thermal shrinkage it was possible to tailor crimp patterns on electrospun fibers. With slight modifications in the process, a few structural configurations were achieved. In this sense, the developed scaffolds can be defined as a multiscale structure that in practical terms can address more demands and clinical applications. When hMSCs were seeded into wavy scaffolds their spatial distribution appeared more even over time when compared to flat scaffolds. The similarity between dense wavy scaffolds and tendons/ligaments was assessed and proved, as those patterns could mimic the effect of the presence of TGF β (Transforming Growth Factor β).

Conclusions: Crimp patterns can be tailored in electrospun fibers by thermal shrinkage and few structural configurations can be achieved with small changes during fabrication. In this sense, the developed scaffolds can be defined as multiscale structures that in practical terms can address more demands and clinical applications. By changing the thickness of the scaffold the patterns can go from single fiber curling to surface undulations. While single fiber curling might have an effect on cellular ingrowth contributing to a more even spatial distribution of cells, surface undulations may contribute to cellular differentiation as cells become more elongated. The similarities

between these patterns and biological patterns in tendons and ligaments were tested, showing that the scaffold itself could mimic the presence of TGF β .

Acknowledgements

First of all I would like to thank my supervisor, Honglin Chen, for the initial support when I arrived, for providing me with the tools that I needed to keep up working more independently.

I also would like to thank my supervisors, Prof. Lorenzo Moroni and Prof. Roman Truckenmüller for all the help and guidance, for inspiring me to do more and better.

I would like to thank my supervisor in Portugal, Prof. Hugo Ferreira, for answering all my questions and helping me with this dissertation.

I also present my thankfulness to Prof. Clemens van Blitterswijk for giving me the opportunity to develop my master thesis at the Department of Tissue Regeneration of the University of Twente.

To Dr. Hugo Fernandes, thank you for letting me explore a new side of the project and thank you for providing everything to help me with it.

Sara Neves and João Crispim, a special thanks for being my “fake supervisors” and helping me with my daily dilemmas, without them I couldn’t make it!

To the Lorenzo’s Group and TR team for the collaboration and great work environment.

To my old friends that I really missed, all moments I would never forget!

To my new “Enschede Family” that were my companions during half a year. Thank you for making this period one of the best moments of my life, seriously I am really glad that I met you, You made me really Happy!

To my boyfriend that always encouraged me to pursue my dreams and cheered me up when I missed the most what I left in Portugal. Thanks for everything, for the visits and for the surprises, for the conversations, for the laughs, it meant the world to me!

Finally to my family, specially my parents, they were my pillars, my strength and my motivation. For making my dreams come true! I am the happiest daughter in the world for having them as my parents. To my Mom, for ALWAYS being with me; for all the love, comprehension and patience.

This thesis is dedicated to them.

Index

Acknowledgements.....	vi
List of figures	4
List of acronyms	7
1. Introduction	8
1.1.Context	8
1.2.Aim and outline of the thesis	9
1.3.Electrospinning.....	10
1.4.Principles and conventional setup	10
1.5.Bending and buckling instabilities.....	11
1.6.Parameters	11
1.7.Advantages and disadvantages of this technique.....	12
1.8.Increasing three-dimensionality within the scaffold	13
1.9.Cellular ingrowth	14
1.10.Stem cells and mechanotransduction	15
1.11.Requirements for tendon/ligament scaffolds.....	16
2. Hypothesis.....	19
3. Materials and Methods	20
3.1.Novel approach to curl fibres.....	20
3.2.Fabrication of PA-PLA scaffolds.....	20
3.3.Fabrication of PA-PLA scaffolds with different orientations.....	21
3.4.Fabrication of PA-PVA-PLA scaffolds.....	22
3.5.Fabrication of multiscale scaffolds.....	23
3.6.SEM observation	23
3.7.Quantification and statistical analysis of the wavelength and amplitude	24
3.8.Cell seeding (hMSCs)	24
3.9.Cell seeding (MLEC)	24
3.10.Methylene Blue assay for hMSCs seeded scaffolds	25
3.11.Fluorescent labelling and imaging for hMSCs seeded scaffolds	25
3.12.Cryosectioning of PA-PLA scaffolds seeded with hMSCs	26

3.13.	Depth of infiltration analysis and quantification of PA-PLA scaffolds seeded with hMSCs	26
3.14.	Presto Blue assay for MLEC seeded scaffolds	26
3.15.	Luciferase assay and DNA assay for MLEC seeded scaffolds	26
4.	Results	28
4.1.	PLA film characterization	28
4.2.	Novel approach to curl fibers	29
4.3.	Influence of deposition's orientation on curled patterns	30
4.4.	Sacrificial fibers	31
4.5.	From single fiber curls to multiscale waves	33
4.6.	Different types of structures	35
4.7.	Pilot cell study	37
4.8.	Cellular ingrowth	40
4.9.	Tendon /Ligament similarities	42
5.	Discussion	46
6.	Similarities between native tissues and the multiscale scaffold	52
7.	Conclusions and future work	54
8.	Attachments	56
9.	References	58

List of figures

Figure 1 Conventional electrospun setup.	10
Figure 2 a) Crimp pattern present in the Achilles rat tendon ⁵⁵ b) Groovy pattern present in patellar tendon ⁵⁶ c) Collagen crimping effect. ⁵⁷	17
Figure 3 Schematics with basic steps of production and application of thermal shrinkage. a) corresponds to the electrospinning, where the PA is electrospun on top of a PLA film; b) represents the sample before the thermal shrinkage, step c), and d) represents the shrunk sample. a.1) and a.2) depicts the possibilities between random and aligned fibers and c.1) represents the structure used to prevent samples from losing their flatness during shrinkage inside the oven.	21
Figure 4 Schematics on how to get different orientations by changing the position of the film over the electrodes.	21
Figure 5 Setup including a mandrel to enable simultaneous electrospinning of two polymers.	22
Figure 6 The first graph represents the percentage of PLA shrinkage obtained at different temperatures and periods of shrinkage. The second graph shows in more detail the film behavior at 75° C. As standard it was established 1 minute at 75° C with a shrinkage of 60%.	28
Figure 7 Illustration of how the samples were cut and labelled from the whole PLA sheet.	28
Figure 8 SEM pictures depicting the before (a and b) and after (c and d) the thermal shrinkage. In d) is possible to see a 3D coil which was not common. Scale bars, 2 µm.	29
Figure 9 Measurements were made to check fiber diameter a) before and b, c) after shrinkage. Scale bars, 2 µm.	29
Figure 10 Comparison between the fibers deposited in different directions before and after shrinkage. Scale bars, 5µm.	30
Figure 11 The wavelength and amplitude were measured for each configuration (parallel, diagonal 1 and diagonal 2) present in y-axis. The differences were statistically significant, ***p-value<0.001, **p-value<0.05 and *p-value<0.1.	30
Figure 12 SEM pictures of PA-PVA simultaneously electrospun scaffolds before and after immersion in water and consequently removal of the PVA. Scale bars, 500µm.	31
Figure 13 Removal of sacrificial fibers on low density scaffolds. The order of deposition was varied, in a) the first layer was PA and in b) the first layer was PVA as it is explained in the schematics. The SEM pictures show before and after immersion and consequently removal of the PVA. Some differences are visible in the crimp pattern. Scale bars, 100µm.	32

Figure 14 The graph in a) shows wavelengths and amplitudes measured (y-axis). The data was divided into 3 categories: PA-PVA which corresponds to PA as first layer of deposition and PVA as second layer and PVA-PA which corresponds to PVA as first layer and PA as second layer, p-value<0.001. The distinction between big loops and small loops is explained in the b) figure, where the same fiber has two different curls that were measured in separately. In b) is also described how the parameters were measured. Scale bar, 20µm.	33
Figure 15 Topographical evolution as the time of deposition increased. The samples where fibers were deposited perpendicular to the axis started to show waves rather than only curls after 9 minutes of deposition whereas the perpendicular samples showed waviness after 5 minutes. Scale bars, 500µm.	34
Figure 16 A graph depicting the thickness of samples with fibers deposited perpendicular or parallel to the shrinkage axis, according to time of deposition. In yellow is marked the transitional points from whether the scaffold more than curls evidence waviness.	35
Figure 17 Diagram showing the possibilities created with these scaffolds and the thermal shrinkage based on the type of film used.	36
Figure 18 a) and b) Shows the extra polymer found when the scaffolds are free from the electrodes that can influence the shrinkage pattern of the scaffold.	36
Figure 19 Figure a) shows an specimen of the floating wavy scaffold before and c) after shrinkage. In c) is showed a SEM picture of them. Scale bar, 100µm.	37
Figure 20 Methylene blue assay enables the visualization of cells and its distribution across the surface. a) corresponds to PLA film without fibers, b) corresponds to the shrunk PA scaffold and c) corresponds to not shrunk PA scaffold. Scale bars, 0.1 mm.	37
Figure 21 The SEM pictures shows cells on flat and wavy scaffolds and the differences found in their morphology. Flat scaffolds revealed spread and larger cells whereas wavy scaffolds showed more elongated and spindle-like cells. Scale bars, 200 µm and 100 µm.	38
Figure 22 Series of SEM magnifications showing a cell on a tighter wavy scaffold bridging from one peak to the other. In these type of scaffolds cells tend to appear more elongated. Scale bars, 1mm, 200µm and 10µm, respectively.	38
Figure 23 SEM magnifications of two examples where the looser waves tend to induce cell spreading. Scale bars, 200µm and 50 µm in the upper set and 1mm and 100 µm in the lower set of images.	39
Figure 24 Cell entrapment in between electrospun fibers. Scale bars 10 µm and 5µm (bottom right.	39
Figure 25 Dapi and Phalloidin merged images from top view in flat and wavy samples. Scale bars, 200 µm.	40

Figure 26 Bright field and DAPI images for two time points and respective conditions. The nuclei are labelled blue. Scale bars, 200 μ m.	40
Figure 27 Grid created in ImageJ to measure cell infiltration along the cross-section. The numbers represent the bins, 1 corresponding to the top and 5 to the bottom.	41
Figure 28 The graph shows the doubling effect in thickness registered after shrinkage. p-value <0.05	41
Figure 29 The two graphs represent the amount of cells present in each depth section of the scaffold. For each scaffold region, the number of cells was counted and normalized to the total cell number present in the sample and the thickness of the sample, therefore.	41
Figure 30 The Presto Blue graph shows the cell viability over time for each condition. The Luciferase data reveals the amount of light produced in each condition. Differences between <i>cells</i> and <i>tgf</i> samples when compared to others are due to differences in cell density	43
Figure 31 The Presto Blue graph shows the cell viability over time for each condition. The Luciferase data reveals the amount of light produced in each condition. Note that the results were not expected to be like this, the difference between flat and wavy samples is not significant.	44
Figure 32 The graphs show the result for the Luciferase assay with and without DNA normalization for both time points.	44
Figure 33 DNA content of the third trial of the tendon/ligament experiment.	45
Figure 34 Figure a) show a SEM image of a ciliary body and c) a SEM image of the iris (scale bars, 1 mm; <i>from www.sciencephoto.com</i>), compared to b) and d) SEM pictures of two different configurations of the multiscale scaffold.	52
Figure 35 Figure a) shows artery wall composed by curled elastin bundles separated by collagen (scale bar, 25 μ m) compared (<i>from www.sciencephoto.com</i>) to b) a shrunk low density scaffold with curly fibers (scale bar, 20 μ m).	53
Figure 36 SEM image of tracheal wall displaying a crimp pattern (<i>from www.sciencephoto.com</i>) compared to one of the forms of a high density shrunk scaffold.	53

List of acronyms

ESP Electrospinning

ECM Extracellular matrix

HFIP Hexafluoroisopropanol

hMSC Human mesenchymal stem cell

MLEC Mink lung epithelial cell

PA PolyActive®

PAI-1 Promoter activator inhibitor 1

PASA Polyaspartic acid

PEDOT: PSS – PVP Poly(3,4-ethylenedioxythiophene :poly(styrene sulfonate) – poly(vinyl pyrrolidone)

PEO Polyethylene oxide

PLA Polylactic acid

PS Polystyrene

PVA Polyvinyl alcohol

PVDF Polyvinylidene fluoride

PVP Polyvinylpyrrolidone

TGF Transforming growth factor

1. Introduction

1.1. Context

Since there are hundreds of people waiting for all sorts of transplants, and the number of existent donors is not enough for the demand, tissue engineering appears as a plausible solution for such shortage of donors.

Tissue engineering is an emerging field in which materials and cell biology are combined, in presence or absence of biological factors, to recreate the natural process of tissue formation by assembling cells onto scaffolds. Scaffolds are supposed to mimic native tissue. In order to produce scaffolds better mimicking the native environment, it is fundamental to understand cell behavior and how cell-scaffold interactions are regulated before translating them into further scaffolds improvements¹.

Electrospun scaffolds have been used because of their simple production method and their ability to recapitulate key physic-chemical features of native tissues². Fiber alignment, which can be easily obtained with electrospun meshes, is also really appealing for tissue engineers. The hope that fiber alignment could orientate and guide cells to organize their ECM (extracellular matrix) is one of the main reasons to apply such scaffolds whenever a specific tissue organization is needed.

Electrospun scaffolds have been applied to almost every field in tissue engineering. With a few adjustments or complements and the results seem to be positive. Synthetic electrospun scaffolds were tailored in terms of porosity and pore size for dermal tissue engineering³. Aligned electrospun nanofibres provided an instructive microenvironment for cells to differentiate into the teno-lineage⁴. Osteogenic differentiation had been studied on plain electrospun scaffolds and on electrospun scaffolds with mineralized surfaces, and the results showed that fiber alignment affects proliferation and differentiation^{5,6}.

Despite all trials made so far, electrospun scaffolds still need to be optimized in terms of their capacity to support cell infiltration and in their degree of mimicry with respect of native tissues.

1.2. Aim and outline of the thesis

The overall aim of the work presented and discussed in this thesis was to create a new scaffold with increased three-dimensionality to improve cellular migration and induce some differentiation.

The present thesis is comprised of seven chapters, as described below.

The first chapter introduces the context in which the project is inserted, the overall aim and the outline of the thesis. The Electrospinning technique is also introduced. Here, the basic functioning principles, the inherent instabilities, and how they affect the final product, are explained. The parameters and their effect on fibers are discussed as well as the advantages and disadvantages of the technique. The novel approach used in this thesis is compared to the already existent ones. The interactions between cells and the scaffold and how these can influence cellular fate is presented and related to how cell shape can influence differentiation. The problem of poor cellular infiltration in electrospun scaffolds is discussed, as well as some of the attempts to solve it. Finally, there is a segment about tendon and ligament engineering.

In the second chapter, the hypothesis for this thesis is presented.

In the third chapter, the materials and methods are presented, while the fourth chapter comprises the results obtained in all experiments performed during this project.

The fifth chapter discusses the approach developed to create curls and imprint more free volume inside electrospun scaffolds. The wavy scaffolds are compared to flat ones in order to see if the cellular infiltration was improved by curling the scaffold fibers. The ability of the wavy scaffold created to mimic the presence of TGF β and induce differentiation on transfected cells highly sensitive to this growth factor is also discussed.

The sixth chapter, “Similarities between native tissues and the multiscale scaffold”, appears as a motivation chapter presenting a few examples of resemblance between some “modes” of the multiscale scaffold and native tissue. This chapter acts as an inspiration for future work. Finally, the seventh chapter, “Conclusions and future work”, summarizes the overall project and presents some ideas for the future.

1.3. Electrospinning

For the last century researchers have been revisiting old processes, electrospinning in particular. This technique was started by J. F. Cooley in 1900 and after an important contribution of Sir G. Taylor, who came up with a mathematical model of the conical shape formed at the beginning of the ejection stage (Taylor's cone), it was intensively developed in the mid-1990s by *Reneker* and his group^{7,8}. The interest in nanoscience and nanotechnology arose and researchers started to realize the potential of nanofibre production. Nanofibres with their high surface area to volume ratio could improve technology as they behave as a dynamic system where the pore size and shape can change, unlike conventional structures and therefore they can be applied at several new areas. Electrospun fibres are also used in protective clothing, filtration and nano-electronics, besides tissue engineering⁹. Apart from other methods of fabricating nanofibres, electrospinning is by far the most versatile, flexible and straightforward. Researchers have been electrospinning polymers, composites, semiconductors and ceramics. In terms of laboratory demands, the setup is quite simple and the process is entirely physical⁷.

1.4. Principles and conventional setup

The conventional setup for electrospinning includes three major components: a high-voltage supply, a syringe with pumping system and a collector plate as shown in figure 1; through the application of an electric field, a charged polymer solution is created. This solution held inside a needle connected to a syringe undergoes three main forces: gravity, mutual charge repulsion and surface tension. The gravity influence is easy to understand but does not play an important role. Surface tension is the main force preventing the drop to form and fall, so the polymer stays inside the needle. The charge repulsion causes a force directly opposite to the surface tension. Hence there is a competition between these two forces and only when the electric field reaches a critical point and the electric repulsion overcomes the surface tension, the hemispherical surface of the polymer solution forms a conical shape (Taylor's cone) and the ejection of the polymer is initiated from the apex of the cone^{10,11}.

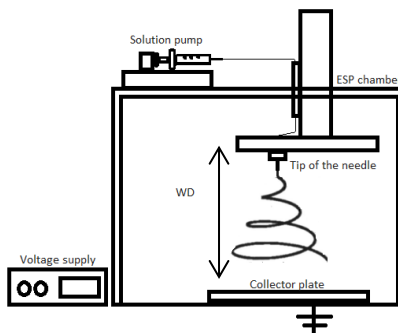


Figure 1 Conventional electrospun setup.

As the solution travels in air, the solvent starts to evaporate, the polymer becomes solid and the fibre is formed. The final stage occurs with the collision of this fibre on a metal collector, which catches the product formed by electrospinning. Deposition's pattern of electrospun jets results from two phenomena: electrical bending and mechanical buckling. The difference between them is clear when comparing their deposits on a collector plate.

1.5. Bending and buckling instabilities

Charged jets don't follow a straight path from the ejector to the collector; several studies were done concerning how electrostatic forces affect a solution and how this behaviour is reflected during electrospinning. The easiest instability to be shown present in electrospinning was the electrical bending as it is visible to the naked eye, but a few years later it was shown that if the jets reach the collector in a straight trajectory they might experience some mechanical buckling resembling the one discovered by Euler, related to compressed elastic bars. These instabilities are reflected in the patterns created during the polymer collection ^{12,13}.

Patterns associated with bending instabilities correspond to larger loops, whereas for buckling the pattern appears to be smaller. Buckling may or may not occur along bending because these phenomena have different natures. Bending instability is due to mutual repulsion of excessive charges within electrospun jets and previous work showed that there are at least three levels of this kind of instability ¹³. Buckling is a consequence of the vertical impact of fibres on a steady collector plate ^{12,14}. This causes a longitudinal compressive force that induces a fibre deformation. Thus macroscopic coils observed in an electrospun sample are due to electrical bending and microscopic curls result from mechanical buckling ¹².

1.6. Parameters

Electrospinning depends on several parameters that can be categorized as polymer solution properties, processing variables and ambient parameters.

The properties of the solution are polymer molecular weight, viscosity, conductivity, surface tension and dielectric effect of the solvent. Molecular weight is one of the most important factors during ESP. Polymer weight represents the length of the polymer chain and this determines the amount of entanglement of polymer chains in the solvent, which is related to polymer viscosity. Additionally, chain entanglement increases with polymer concentration making the solution more viscous^{9,15}. The interaction between the solution and charges on the jet will determine the fibre diameter obtained. When the viscosity is too high it may reduce the probability of second-jet formation leading to larger fibres. When the opposite happens it may result in fibres with smaller diameters¹³. As the initiation of ESP requires the charged solution to overcome its surface tension

the idea is to use a solvent with lower surface tension in order to get smooth fibres, avoiding beads^{11,16}. The stretching experienced during the ejection of the solution is caused by repulsion of the charges at the solution's surface. Thus, if the conductivity increases, more charges are carried and the fibres will be more elongated, smoother and with smaller diameters⁹.

Processing variables include: voltage, feedrate, working distance (between the tip of the needle and the collector), type of collector and diameter of the needle. As the application of high voltage is one of the requirements for ESP, the change of this parameter will have a great impact on the result. As the Coulombic repulsive forces in the jet are responsible for stretching the viscoelastic solution, when voltage is increased the greater amount of Coulombic forces will lead to a reduction in fibre diameter^{9,17}. The feedrate determines how much solution is available at the tip of the needle and therefore it has an influence on how stable the Taylor cone is. When this parameter is increased, more solution is drawn away from the needle and consequently the diameter increases⁹. The most relevant property of the collector is its electrical conductivity. With conducting collectors, fibres can be packed closed together as charges are dissipated while with non-conducting collectors accumulate charges which may result in 3D structures due to the repulsive forces^{9,17}. The internal diameter of the needle used has also an impact in how the fibres come out: if the needle has a small diameter the fibre comes out with a smaller diameter as well. Using a smaller needle can reduce the clogging and the amount of beads⁹. The working distance (distance between the tip of the needle and the collector) has an effect on the time of flight (TOF) of fibres and electric field strength. TOF increases with distance leading to a decrease in fibre diameter⁹. The tunability of these parameters is limited and when it is pushed too far from the normal values it can result in bead formation (excessive increase of voltage) or fibres can be fused together on the collector (excessive increase of feedrate or small working distances).

Temperature, humidity and pressure inside the chamber are ambient parameters. The temperature can influence the evaporation rate and reduce viscosity, at higher temperatures fibres look more uniform, concerning the diameter, due to a decrease in viscosity and increase in solubility. Humidity has a role dictating the evaporation rate of the solvent, lower values may lead to quick evaporation time. When the pressure is below atmospheric level, the solution will have more chances to flow out of the needle causing unstable jet initiation⁹. Usually the parameters changed are the voltage, feedrate and working distance¹⁰.

1.7. Advantages and disadvantages of this technique

Electrospinning is a straightforward and cost effective technique used to produce fibrous scaffolds. Fibre alignment and pore size can be adjusted through the parameters mentioned above, allowing the fabrication of highly interconnected porous structures with dimensions that may mimic native cellular environments. However, one of the main challenges for the application of these scaffolds in tissue engineering is the lack of cell infiltration through the meshes mainly due to the inherent small pore sizes¹⁸. There is a strong correlation between fibre diameter and

pore size; if the fibres are in the nano- or microscale, consequently the pores will be in the nano- or microscale¹⁹. The goal is to create an electrospun scaffold with nanofibres and macropores which in theory would enhance cell colonization.

1.8. Increasing three-dimensionality within the scaffold

One of the major approaches in tissue engineering is the combination of a scaffold with cells in order to generate or regenerate a tissue. The first approaches were taken with 2D cultures which were easier to establish and control, but in fact, in order to recreate a tissue/organ a better and more realistic approach is to start with 3D scaffolds, designed to be more similar to the target as possible. It is not simple to achieve this kind of perfection, maybe because simple methods lack in precision and more complex structures can only be fabricated using nanotechnology. Currently, the trend is to go back a few decades and look at the methods used, generally way simpler than most recent ones, and adjust them to the nowadays demands. As it was described before, the electrospinning is one of them. Electrospun fibers are straight by nature and beside the inherent instabilities they do not show variation in terms of structure and conformation.

Driven in particular by electronics, researchers are trying to reshape electrospun fibers and one of the chosen configurations is the coil. For instance *Sun et al.* have created poly(3,4-ethylenedioxythiophene:poly(styrene sulfonate)–poly(vinyl pyrrolidone (PEDOT:PSS–PVP) curled conducting polymer arrays using a conventional electrospinning setup plus harmonic motion of the spinneret (reciprocating-type electrospinning). The structure created could be stretched reversibly making an alternative for a stretchable strain tensor²⁰. Keeping the conventional setup, changing only the collector plate for a nail tip collector, it was possible to create curled fibres. This happened because as the collector has a small area the electric field converges to it, while bending. So the fibres were forced to bend. As the voltage reached values around 40kV bending perturbations rose, thus increasing the chances of curling. As it was mentioned before, there are buckling and bending instabilities and at higher voltages mechanical buckling becomes dominant^{12,21}. The only drawback of this method is that with higher voltages the possibility of bead formation is higher, changes in the crystallinity of the polymer might occur and this may change the way fibres pack together⁹.

Based on the piezoelectric property of Polyvinylidene fluoride (PVDF), *Sundaray et al.* found that when PVDF was electrospun on top of aluminum foil the structure behaved like a piezoelectric bimorph bending under the influence of the electric field²².

More elaborate alternatives were taken including the electrospinning of a composite of one conducting material (Polyethylene oxide - PEO) and one non-conducting material (Polyaspartic acid - PASA), which coiled due to viscoelastic contraction upon partial neutralization of the charged fibres²³. Another example is the UV irradiation of only half of the outer shell of

electrospun fibres producing asymmetric fibres (*Janus* fibres) with a soft core and stiff outer half-shell. It was observed that when the fibres were left in relaxation (eliminating the stress induced by the two sides of the collector) fibres started to curl forming helices and only when those helices were stable the surface started to wrinkle (only on the irradiated part) ²⁴. *Guoqing Chang* and his group develop a method to produce copper metal coils based on the electrospinning of PVP and copper cations around an axis. As the fibre was negatively charged and it could not discharge on the grounded parallel collectors that weren't good conductors, it was attracted to the positively charged rotating axis coiling there. Nanoribbons were formed after calcination and reduction in H₂. All these approaches addresses the question of creating non-linear fibers but none is really simple and cost-effective to be used on a regular basis.

1.9. Cellular ingrowth

The assembling of cells within a scaffold is not a straightforward process. One of the biggest problems of electrospun scaffolds in tissue engineering is the lack of cellular infiltration due to fiber density. Recent work on this subject focused, basically, on three approaches in order to increase the permeability to cells, promoting their migration towards the center of the scaffold: i) patterned collectors, ii) salt leaching, and iii) sacrificial fibres.

The utilization of patterned collectors, depending on their design, can be an easy way to control the density of deposited fibres. Based on conducting/ non-conducting properties, the regions of the collector that correspond to holes or indentations will have a less amount of fibres in comparison to the rest. Hence, if there are fewer fibres, pores can be bigger and cellular infiltration is improved, but the scaffold would not have a homogenous pore network. The existence of dense zones of fibres and zones of lower fiber density lowered the mechanical properties of the pattern scaffold, under both static and dynamic conditions ¹⁹.

The addition of particles to create spaces between fibres is another alternative to create more porosity in fibrous scaffolds. During electrospinning the particles can be added between fibres and after that removed leaving behind the pores. One of the problems associated with this is the delamination of polymer sheets, because there are not enough fibres to hold all layers together²⁵.

Finally, the last approach presented is the selective removal of sacrificial fibres. Two polymers with different properties are electrospun, one with a slow-degrading rate and the other one water soluble. After simultaneous spinning, the mesh is placed in an aqueous environment and the water soluble polymer is removed leaving behind empty spaces which increase porosity ²⁶.

1.10. Stem cells and mechanotransduction

The use of stem cells not only opens up the potential to produce safer patient-specific tissues but also allows the creation of more complex structures. Stem cells, including embryonic, foetal and adult ones have two important features: the ability to self-renewal and the ability to differentiate into multiple lineages. The main difference between the three types mentioned is the differentiation potency; embryonic cells are pluripotent whereas adult cells are only considered multipotent²⁷. Ethical issues and availability make adult stem cells more likely to be used in Tissue Engineering²⁷.

Adult stem cells include mesenchymal, epithelial, neural and hematopoietic stem cells. Mesenchymal stem cells (MSCs) or stromal, can be found in the bone marrow and have been shown to differentiate into various cell types including osteoblasts, chondrocytes, adipocytes, smooth muscle cells and, controversially, neurons. However, in most of the cases these cells are led into a specific lineage through soluble factors such as dexamethasone for osteogenesis²⁸, insulin for adipogenesis²⁹ and hydrocortisone for smooth muscle cell differentiation³⁰. There is now compelling evidence that the topography can produce similar effects regulating cell fate^{30,31}. Scaffolds contain important information for cells in their topography, size, shape, and porosity, cues that can range from the nano (as the collagen bundling) to the macroscale (the shape and size of the organ itself)³².

Ideally, the scaffold should be a functional and structural biomimetic of the native extracellular matrix and support multiple tissue morphogenesis. It was already shown that electrospun fibers within scaffolds morphologically resemble collagen fibrils and can promote positive responses from seeded cells. Beyond that, they can direct hMSCs into different lineages if supplemented with the right soluble factors and adjusted anisotropy^{33,34}. Another study explored the feasibility of utilizing electrospun silk fibroin scaffolds for vascular grafts and the results suggested the potential of these scaffolds for this purpose as they supported vascular cell viability, maintained cell shape and promoted cell reorganization. Previously, it was shown that these scaffolds can be rolled into tubular structures with enough mechanical integrity to support vascular pressures³⁵.

In order to survive cells rely on interactions with other cells and their surroundings. When a scaffold is seeded with cells, it should undergo a process of remodeling. During repopulation and expansion, cells take advantage of the scaffold through a series of mechanisms that allow them to sense the surroundings. This capacity to sense the environment is known as mechanotransduction. Yet, our understanding of the mechanisms behind mechanotransduction is still limited. The general idea is that the cell behaves like a transducer converting mechanical cues into biochemical responses which results in gene- and protein level modulation.

Cellular fate is regulated by cell-generated tension that is enabled through cell-mediated degradation of the matrix³⁵. This degradation is accompanied by a drastic change in cellular shape which is believed to influence the stem cell commitment, the process by which a cell decides its fate, differentiating. While differentiation may cause changes in cell shape, several studies

highlighted that changes in cell shape themselves can alter the differentiation of pre-committed mesenchymal lineages.³⁶ The shape that a cell assumes depends on the assembly of focal adhesions and cytoskeletal organization. Focal adhesions are formed by integrins binding to their ligands in specialized clusters which ensure substrate adhesion as well as directed assembly of actin filaments and signaling components³⁷.

When MSCs differentiate into osteoblast they become elongated and spread. Osteogenic differentiation appears to require stiff and spread actin cytoskeleton. This is also related to plating cell density; in lower densities cells have more spatial freedom to stretch themselves, thus increasing their osteogenic potential. The more spread the cells the more RhoA is expressed, a small GTPase known to regulate the actin cytoskeleton³⁶.

Adipogenesis implies a cytoskeleton that does not have much organization or tension. Since adipocytes are usually round, they do not require an organized cytoskeleton and prefer high plating densities which confines cells preventing the spreading³⁸.

The chondrogenic requirements are similar to adipogenic ones as cells share the same cytoskeleton configuration. *In vivo*, chondrocytes assume different morphologies without significant differences in the cytoskeleton organization, in articular cartilage, chondrocytes exhibit a spherical (intermediate zone), elongated (superficial tangential zone) and oblong shape (deep zone). Therefore, the factor that distinguishes these two lineages must be related to chemical signaling and not so much cytoskeleton related.

Although cytoskeleton organization seems to be the most important structural aspect, focal adhesions are crucial for osteogenic differentiation whereas chondrogenesis and adipogenesis are encouraged by preventing focal adhesion attachment³⁹. Despite the morphology, focal adhesion configuration also has a role on stem cell differentiation. Two cells may appear an elongated cell shape but only one of them may have elongated focal adhesions, with the right substrate design is possible to discard one effect over the other⁴⁰.

1.11. Requirements for tendon/ligament scaffolds

Tendon and ligament injuries are a common clinical problem in either workplace or sports. There are about 30 million annual tendon and ligament injuries worldwide⁴¹. These injuries can be acute or chronic. Acute injuries are primarily caused by trauma, whereas chronic injuries are prone to happen when repetitive mechanical loading below the failure threshold occurs or in case of inflammatory responses⁴².

Tendons and ligaments are able to heal naturally but never to a pre-injury condition owing to the scar formation (they do not regenerate, they form a fibrotic scar) which decreases the biomechanical potential. The loss of mechanical integrity is mainly due to a distorted ECM composition and a misalignment of collagen fibrils in the scar tissue.

Despite all efforts made to improve surgical skills (sutures and anchors), repairing a tendon/ligament is still a difficult task and the results are still inferior⁴³. Thereby, the quest for alternatives includes biological grafting, permanent replacement with artificial prostheses and tissue engineering⁴⁴.

Biological grafting depends on the limited availability, can induce donor site morbidity, can promote disease transmission and has always the chance of being rejected. Permanent artificial prostheses often are not equivalent to the natural tissue. They lack in material durability and sooner or later end up failing mechanically. Tissue engineering represents a more promising but nevertheless an easier approach. The aim is to promote regeneration per se, rather than a replacement. Tendon/ligaments tissue engineering scaffolds must enhance neo-tissue formation by facilitating cell proliferation, by promoting ECM production and by organizing the matrix into functional tissue⁴².

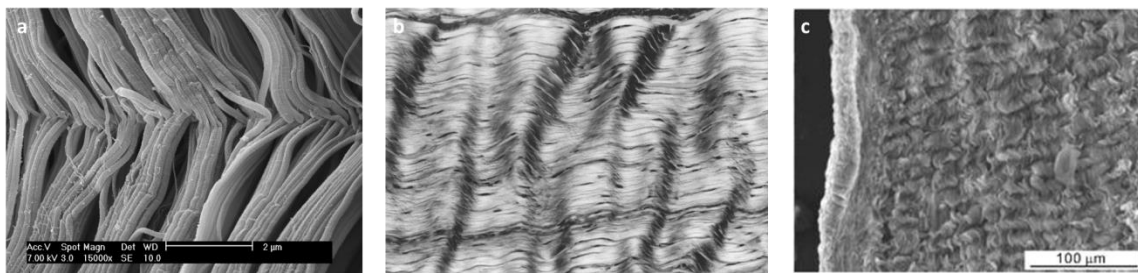


Figure 2 a) Crimp pattern present in the Achilles rat tendon⁵⁵ b) Groovy pattern present in patellar tendon⁵⁶ c) Collagen crimping effect⁵⁷.

Despite the poorly cellular migration, the alignment got in electrospun scaffolds is extremely useful to guide cells, which is important when regenerating tissues that have a high mechanical demand like tendons and ligaments.

Tendons are connective tissues that join muscles to bones. The unique biomechanical properties of tendons are mainly attributed to the high level of organization of their extracellular matrix (ECM). Primarily consisting of collagen type I, the ECM of tendons is arranged in a hierarchy of bundles that have different dimensions and which are aligned in a parallel manner in a proteoglycan matrix. The tenocytes are spindle-shaped tendon fibroblasts that arrange themselves in longitudinal rows with numerous sheet-like cells extensions connected to the ECM⁴².

Ligaments are similar to tendons, they are all connective tissue but, differently, ligaments connect bones to other bones. Ligaments usually refer to a band of tough, fibrous and dense regular connective tissue bundles made of collagen fibers. The connection between a ligament and a bone forms a joint.

Tendons and ligaments mechanical properties are dependent on the collagen fiber diameter and orientation⁴⁵. The collagen fibrils are parallel to each other and closely packed, but show a wave-like appearance due to planar undulations, or crimps, on a scale of several micrometers⁴⁶. In

tendons, the absence of hydroxyproline and proline residues allows flexibility and consequently the development of crimps ⁴⁷.

There is a lack of understanding on natural tendon/ligament development, specially the process of cells condensation leading to a cellular pellet; the formation of ectopic bone (calcium deposition in soft tissues when a neo-tissue is implanted) and tendon-specific markers are still unknown. While not truly tendon-specific, Scleraxis (Scx) is one marker that may be necessary for normal tendon formation but there is a study suggesting that Scx is expressed in many tissues including muscle and heart, Sox9 is a transcription factor important (not exclusive) for chondrogenesis ⁴¹. The balance between both markers, Scx and Sox9, will determine tendon vs cartilage cellular fate, respectively ⁴³.

A recent approach on tendon engineering is the recreation of the natural topography and it seems that the recreation of tendons microenvironment could be sufficient to induce tenocytic differentiation of mesenchymal stem cells ⁴⁸. There is a lot of investigation on the application of electrospun scaffolds to induce tenogenesis as the fibers seems to conduct cells and ECM into a aligned formation ^{4,49}. Some of the studies combine cyclic loads or compressions in order to induce matrix remodeling and the expression of fibrocartilage markers ⁵⁰.

2. Hypothesis

Since the application of electrospun scaffolds in tissue engineering has a few drawbacks, a novel approach to electrospun fibers was developed.

Through thermal shrinkage, electrospun fibers were curled. This simple method could geometrically modify fibers and therefore create and increase the free volume within an electrospun scaffold when compared to the conventional straight fibers. As the film used was mono-oriented, changes in curly patterns would be likely to occur, thus different configurations were tested, and amplitude and wavelength were measured.

In order to increase three-dimensionality, the principle of selective removal of sacrificial fibers would enable the formation of 3D curls. The technique consisted in electrospun two different polymers and then remove one of them (a water-soluble polymer) leaving a structure with increased porosity. A non-flat scaffold would have more free-volume which would allow cells to move easily. Hence, cellular infiltration would be improved making electrospun scaffolds better candidates for tissue engineering.

The shrinkage of the scaffolds would change their topography from a flat surface into a wavy surface. Knowing beforehand that tendons and ligaments have crimps and undulations in their structure, and that their collagen is organized in parallel bundles, it seemed possible to exist a resemblance between natural ligaments and tendons and these scaffolds. This structural similarity could be sufficient to induce some differentiation in cells and mimic the effect of TGF β .

3. Materials and Methods

3.1. Novel approach to curl fibres

Earthfirst®PLA TDO1 shrink films were selected for their mono-orientation. This provides high shrinkage across one direction and little or no shrinkage in the opposite direction.

The fabrication process of this kind of films consists of stretching the polymer when it is warm in order to orient the chains from their natural random orientation. After stretching, the properties are preserved by cooling down the film until a new reheating will cause it to shrink back towards its initial dimensions. Whenever an oriented polymer is heated, disorientation driven by entropy and elastic forces takes place. This relaxation process releases the stored elastic energy from within the intercrystalline (amorphous) regions which simultaneously underwent shrinkage⁵¹.

Thus, when polymer fibers are electrospun on top of these films, the film reacts to the increasing temperature (in the oven) by shrinking and consequently curling the fibers. Without the film underneath the polymer fibers do not curl. The film enables the fixation of the fibers reducing the degrees of freedom; therefore instead of a change in fiber dimension, fibers experience a modification in shape and structural configuration.

3.2. Fabrication of PA-PLA scaffolds

In this experiment PA-PLA scaffolds were fabricated using the electrospinning technique under optimum conditions (24.4°C and 28.8% of humidity). The polymer solution was prepared by dissolving PA (300PEOT55PBT45², *PolyVation*®) into chloroform/hexafluoroisopropanol (4:1) at the concentration of 20% (w/v) and stirred overnight at room temperature until complete dissolution. The solution was then fed into a 5 ml syringe with a 0.8 mm diameter needle controlled by a syringe pump with a rate of 0.5 ml/h. A high voltage was applied (16kV) to the needle tip held upon a working distance of 15 cm. The fibers were collected on a conducting collector plate (random effect) or on two electrodes (aligned effect) for 5 seconds.

The shrinkage and curling were carried out inside an oven at $75 \pm 1^\circ \text{C}$ for one minute *per* sample. To avoid the undesirable curling of the film itself, an improvised structure with a small void was created and placed on top of the scaffold enabling the shrinkage but keeping the film flattened. This structure was comprised of 3 pieces: 2 microscope slides and one silicon wafer (figure 3, image c.1)

¹ Poly(lactic acid) films.

² A blend of poly(ethylene glycol) and poly(butylene terephthalate).

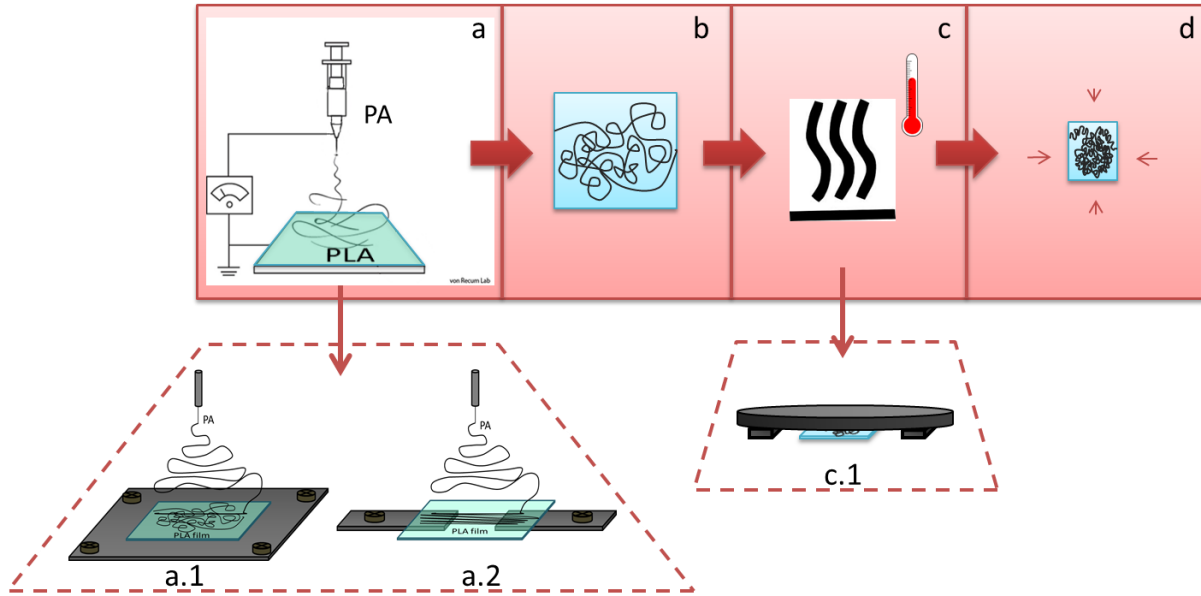


Figure 3 Schematics with basic steps of production and application of thermal shrinkage. a) corresponds to the electrospinning, where the PA is electrospun on top of a PLA film; b) represents the sample before the thermal shrinkage, step c), and d) represents the shrunk sample. a.1) and a.2) depicts the possibilities between random and aligned fibers and c.1) represents the structure used to prevent samples from losing their flatness during shrinkage inside the oven.

3.3. Fabrication of PA-PLA scaffolds with different orientations

The film used was mono-oriented which means that it only shrinks in one specific direction. Hence the effect of curling would depend on how the fibres were deposited on the film.

The scaffolds were produced as described above (figure 3) with the only difference that the film was rotated on top of the electrodes to generate different angles of deposition (figure 4).

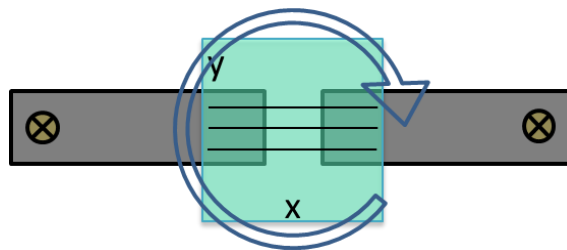


Figure 4 Schematics on how to get different orientations by changing the position of the film over the electrodes.

3.4. Fabrication of PA-PVA-PLA scaffolds

Two different scaffolds were produced: (i) high density (polymers were electrospun at the same time) and (ii) low density (the polymers were electrospun one after the other in a layer-by-layer way).

The PA solution was prepared by dissolving PA (300PEOT55PBT45, PolyVation®) into chloroform/HFIP (4:1) at the concentration of 20% (w/v) and stirred overnight at room temperature until complete dissolution. This solution was then fed into a 5 ml syringe with a 0.8 mm needle controlled by a syringe pump with a rate of 2 ml/h. A high voltage was applied (16kV) to the needle tip held upon a working distance of 13 cm. The PVA solution was prepared by complete dissolution overnight of PVA into EtOH/Demi-water (1:4) at a concentration of 8% (w/v) stirred overnight. The PVA solution was then fed into a 5 ml syringe with a 0.8 mm needle controlled by a syringe pump with a rate of 1 ml/h. A high voltage was applied (16 kV) to the needle tip held upon a working distance of 13 cm.

Part I (high density mats)

To accommodate both needles, the setup was changed and a mandrel³ (300 rpm) was used. The PLA film used (4 x 20 cm) was placed around the mandrel and electrospun for 45 minutes.

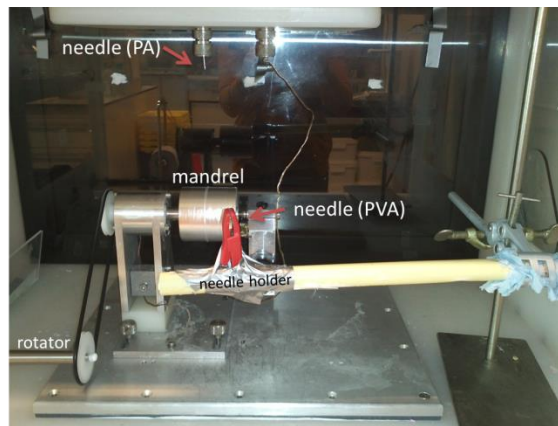


Figure 5 Setup including a mandrel to enable simultaneous electrospinning of two polymers.

The scaffold was cut into 4x4 cm pieces and the shrinkage and curling were carried out inside an oven at $75 \pm 1^\circ\text{C}$ for one minute *per* sample. To avoid the undesirable curling of the film itself, a structure with a small void was placed on top of the scaffold enabling the shrinkage but keeping the film flattened.

³ Cylindrical collector that rotates

Part II (low density mats)

The procedure was the same described in the sections above but for each polymer at a time. A 5 ml syringe with a 0.8 mm needle controlled by a syringe pump with a rate of 2 ml/h. A high voltage was applied (16kV) to the needle tip held upon a working distance of 15 cm for 5 seconds. The order of deposition as well as the orientation were changed to see if there were any differences.

All samples were immersed in water for 45 minutes in order to remove the PVA and let it to dry under atmospheric air.

3.5. Fabrication of multiscale scaffolds

Based on the thermal shrinkage of fibrous electrospun mats it is possible to have different structures only adjusting a few parameters.

2D PA-PLA constructs were produced as described above, using the conventional method of fabrication of PA-PLA scaffolds and applying the selective removal of sacrificial fibers technique.

3D waves and wavy gradients were produced in the same fashion as the 2D PA-PLA scaffolds but with a time of deposition of 10 minutes.

Tight sinusoids were created as the PA-PLA scaffolds, but instead of using a mono-oriented PLA film, it was used a Polystyrene (PS) bi-oriented film, allowing a shrinkage in both directions (x axis and y axis).

Finally the floating wavy mat was created by deposition of PA on top of a rectangular (4 x 2 cm) PLA frame with margins with 0.5 cm.

3.6. SEM observation

To check the morphology of the scaffolds, the samples were sputter-coated with gold and then observed under scanning electron microscopy (SEM) (Philips XL-30) at an accelerating voltage of 10 kV. Ten fibers were taken in to account (five *per* condition) to measure their diameter before and after shrinkage, using the software for the microscope control. Cellular samples underwent dehydration following a sequence of increasing concentrations of EtOH (15 minutes each) from 70% - 100% and finishing with HMDS (15 minutes).

3.7. Quantification and statistical analysis of the wavelength and amplitude

For the low density mats the wavelength and amplitude were measured using Image J, forty fibers were measured for each condition (5 images with 8 fibers each). The wavelength took in to account was the distance between two consecutive peaks; the amplitude was measured as the distance between the maximum and minimum of the wave and then divided by two.

Statistical analysis was carried out to evaluate the statistical significance of the parameters measured. Therefore ANOVA test was used and the significance level was set at $p < 0.05$.

3.8. Cell seeding (hMSCs)

Colony-picked hMSCs (male age 22) were retrieved from the Institute of Regenerative Medicine at Texas A&M University. Briefly, a bone marrow aspirate was drawn and mononuclear cells were separated using density centrifugation. The cells were plated to obtain adherent hMSCs, which were harvested when cells reached 60%-80% confluence. These were considered passage zero (P0) cells. These P0 cells were expanded, harvested and frozen at passage 1 (P1) for distribution.

hMSCs were thawed and expanded in T-flasks till reaching 80% confluence in basic medium (Minimum Essential Medium α [MEM α] containing 10% fetal bovine serum [FBS], 0.2 mM L-glutamine, 0.2 mM ascorbic acid and 100 units/ml penicillin + 100 mg/ml streptomycin).

From 4x4 cm pieces, the samples were punched to fit a 48 well plate (*Thermo Scientific*). After sterilization with Ethanol (2x 15min) and PBS+ Pen/Strep (2x 3min), the scaffolds were incubated in basic medium for three hours.

Cells were seeded with a cell density of 5000 cells/cm² which corresponds more or less to 3000 cells/ml. The cell culture was carried on for 28 days with medium replacement every two days.

3.9. Cell seeding (MLEC)

Mink lung epithelial cells (MLEC), a kind gift from Dr. Daniel Rifkin in the Department of Cell Biology at the New York University School of Medicine to Hugo Fernandes, stably transfected with an expression construct containing a truncated plasminogen activator inhibitor-1 (PAI-1) promoter fused to the firefly luciferase reporter gene. These cells are highly sensitive and specific for TGF- β based on its ability to induce PAI-1 expression⁵².

MLEC (P19) were thawed and expanded in T-flasks till reaching 80% confluence in Dulbecco's Modified Eagle's Medium α [MEM α] supplemented with 10% fetal bovine serum [FBS], 0.2 mM L-glutamine and 100 units/ml penicillin + 100 mg/ml streptomycin). The medium of the control samples was added TGF β 1 (2ng/ml).

From 4x4 cm pieces, the samples were punched to fit a 96 well plate (*Thermo Scientific*). After sterilization with Ethanol (3x 15min) and PBS+ Pen/Strep (3 x 5min), the scaffolds were incubated in the described medium (without TGF β 1) overnight.

Cells were seeded with a cell density of 50000 cells/cm² on the scaffolds and on the tissue culture plate (TCP) as control, the cell culture were carried on for 5 days with two time points: day 2 and day 5. The medium used for the seeding and culture on scaffolds does not include FBS as it may slow down the metabolism and mask the results.

3.10. Methylene Blue assay for hMSCs seeded scaffolds

The methylene blue assay is a quick and simple way to assess the cellular proliferation through estimation of the number of adherent cells present in culture. All samples were washed with demi-water (x2), covered with 400 μ l/well for 30 seconds and re-washed with demi-water a few times. Samples were observed under a stereomicroscope (*Nikon SMZ-10A*)

3.11. Fluorescent labelling and imaging for hMSCs seeded scaffolds

Samples were stained with DAPI (labels the nucleus) and Phalloidin (labels actin filaments). First, they were fixed with formalin for 30 minutes and washed with PBS. Then, 1% Triton x-100 was added and the samples were kept on ice for 10 minutes and rewashed with a phosphate buffered solution (PBS). A bovine serum albumin (BSA) (10mg/ml) solution was added for 60 minutes to block unspecific bindings. After removal of this solution, the Phalloidin (1:60) in 1% BSA/PBS was added for 1 hour at room temperature avoiding light. The Phalloidin was washed with PBS and added the DAPI (1:100 PBS) for 15 minutes, again, at room temperature avoiding light. Finally, all samples were washed with PBS and kept at 4°C in the dark.

Samples were checked under a fluorescent microscope (*Nikon Eclipse E600*). DAPI and Phalloidin pictures were taken and merged afterwards using *Image J*. Bright field images were also taken with this microscope and merged with the DAPI ones to ease the quantification.

3.12. Cryosectioning of PA-PLA scaffolds seeded with hMSCs

In order to get cross-sections, circular samples were cut in half and embedded with *Cryomatrix™* mounting media on mounting blocks with the cross-section facing upwards. Using the *Shandon Cryotome®*, evenly-spaced (80 µm) sections were cut with a thickness of 8 µm.

To avoid polymer auto-fluorescence, the cross-sections were stained with Sudan Black following the following steps: Sudan Black solution was added for 1 hour on a plate shaker, then washed thoroughly with PBS 5 times for 5 minutes each and placed in a new plate.

3.13. Depth of infiltration analysis and quantification of PA-PLA scaffolds seeded with hMSCs

To measure the depth associated with each cell in each cross-section, the pictures were analyzed using Image J. The approach taken was to define the borders of the section and then to create a grid for each image which divided the height of the cross-section in 5 bins, corresponding to regions from the top to the bottom of the scaffold. Cells were counted in each single bin. The measurements were normalized to the real thickness of the sample.

3.14. Presto Blue assay for MLEC seeded scaffolds

The presto blue (live) assay was performed to check cells viability. The medium was removed from the seeded scaffolds and they were washed with PBS. New medium was added with 10% Presto Blue® (*Life technologies™*). It should be included 3 blanks for this assay with only the medium + Presto Blue® solution. Samples should be protected from light and incubated for 2h.

After the incubation period the medium is removed and placed in a 96 black well-plate and read on a *Victor³™* plate reader (*PerkinElmer®*).

3.15. Luciferase assay and DNA assay for MLEC seeded scaffolds

After removing the medium for the Presto Blue® assay, the samples were washed thoroughly with PBS and it was added Lysis Buffer (5x) diluted (5:1) in Milli-Q water. Samples were stored at -80°C for at least 1h.

Past that period, the samples were defrosted on a plate shaker with the *Luciferase Assay Substrate* (lyophilized) needed for the *Luciferase Assay System (Promega)*. From each well, the content was divided: half for the Luciferase assay and the other half for the DNA assay in 2 different 96 white and black, respectively, well-plates.

Luciferase assay: add the Substrate and read the light produced on *Victor³*™ plate reader (*PerkinElmer*®) column by column to ensure that the reaction is still stable (1 min).

DNA assay: using the CyQUANT® cell proliferation assay kit (*Invitrogen*™), to each well it was added Lysis buffer + RNase and left incubating for 1h on the plate shaker, meanwhile a standard curve was prepared using the λ DNA standard. Past the incubation period the CyQUANT® GR dye was mixed with Lysis buffer and added to the samples and the fluorescence was measured on *Victor³*™ plate reader (*PerkinElmer*®).

4. Results

4.1. PLA film characterization

Three different temperatures (65°C, 75°C and 85°C) were tested during different periods of time.

According to these results, standard values for the film shrinkage were set as one minute at 75°C, once it induced a 60 % shrinkage of the PLA film which was long enough to control the process manually (figure 6).

Another important aspect that was decided during this experiment was the orientation of the film, as it came in as an A4 sheet and it had to be cut in 4x4 cm pieces, the shrinking axis was defined as being x-axis and the other as y-axis (figure 7).

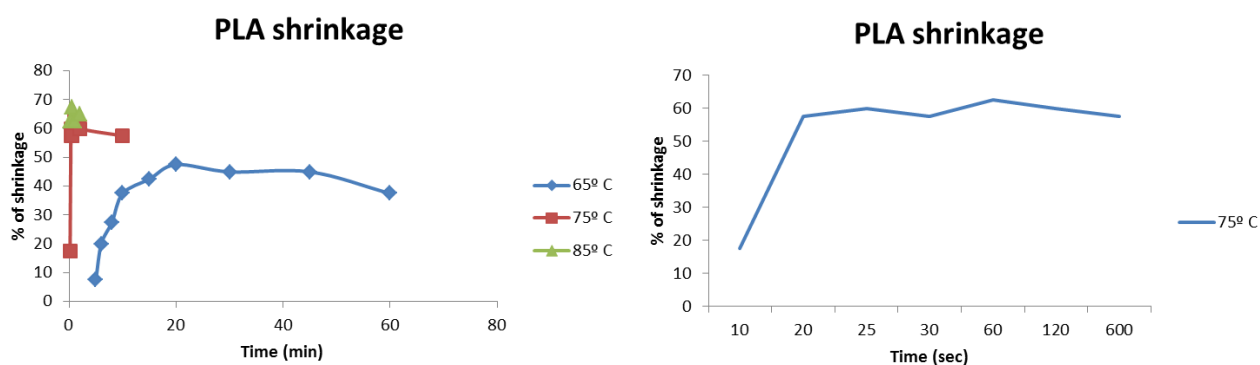


Figure 6 The first graph represents the percentage of PLA shrinkage obtained at different temperatures and periods of shrinkage. The second graph shows in more detail the film behavior at 75° C. As standard it was established 1 minute at 75° C with a shrinkage of 60%.

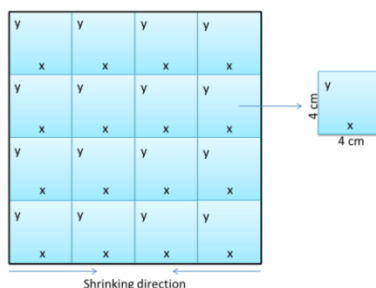


Figure 7 Illustration of how the samples were cut and labelled from the whole PLA sheet.

4.2. Novel approach to curl fibers

The presented method led to formation of mostly 2D curls (figure 8). It was noticeable the difference between before and after shrinking: fibres changed from a linear state to a crimped formation. Figure 9 shows the measurements of the fibre diameter before and after shrinkage. Fiber diameter was 648 ± 308 nm before and 634 ± 259 nm after shrinkage, thus showing no significant influence of the shrinking process on the resulting fiber diameter.

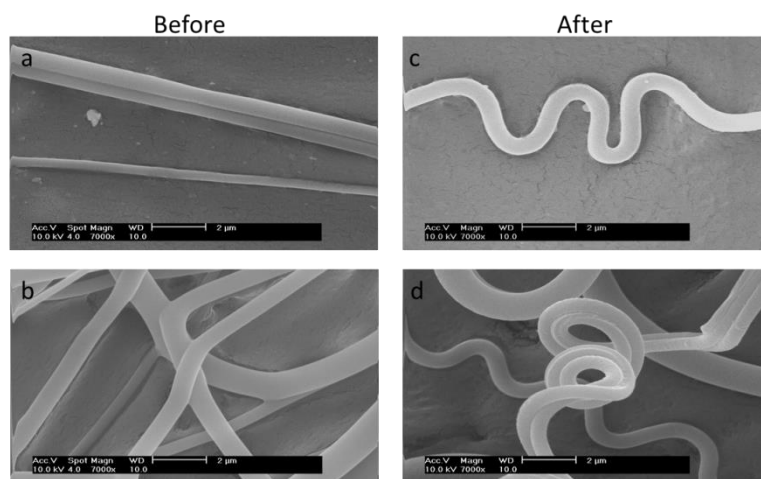


Figure 8 SEM pictures depicting the before (a and b) and after (c and d) the thermal shrinkage. In d) is possible to see a 3D coil which was not common. Scale bars, 2 μ m.

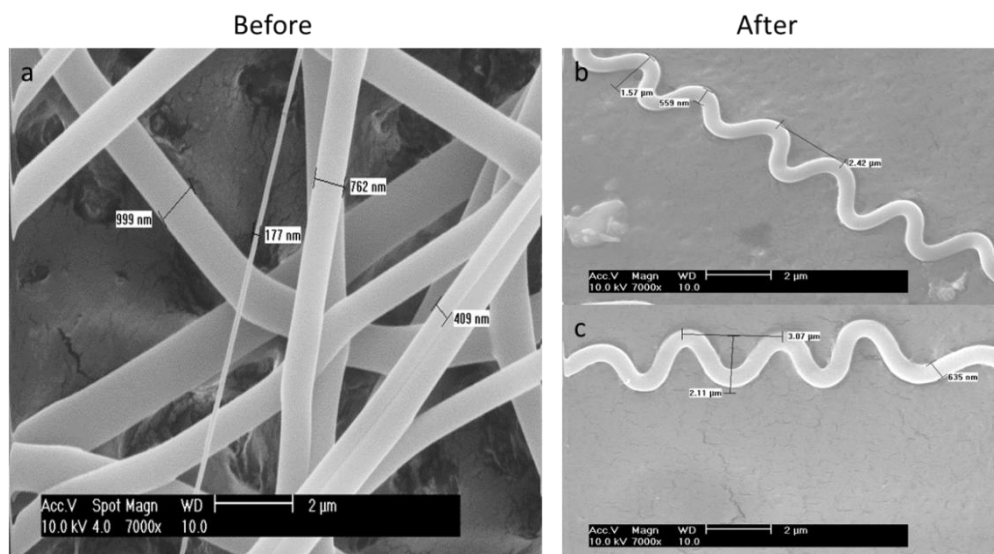


Figure 9 Measurements were made to check fiber diameter a) before and b, c) after shrinkage. Scale bars, 2 μ m.

4.3. Influence of deposition's orientation on curled patterns

Changing the angle of the PLA film during the electrospinning allows the deposition of fibers according to specific orientations. The directions of fibres on top of the film influences the pattern created due to the mono-orientation of the film itself. Figure 10 depicts a comparison between fibers deposited in different directions before and after shrinking. The curls did not appear different. However, the wavelength and amplitude were significantly different.

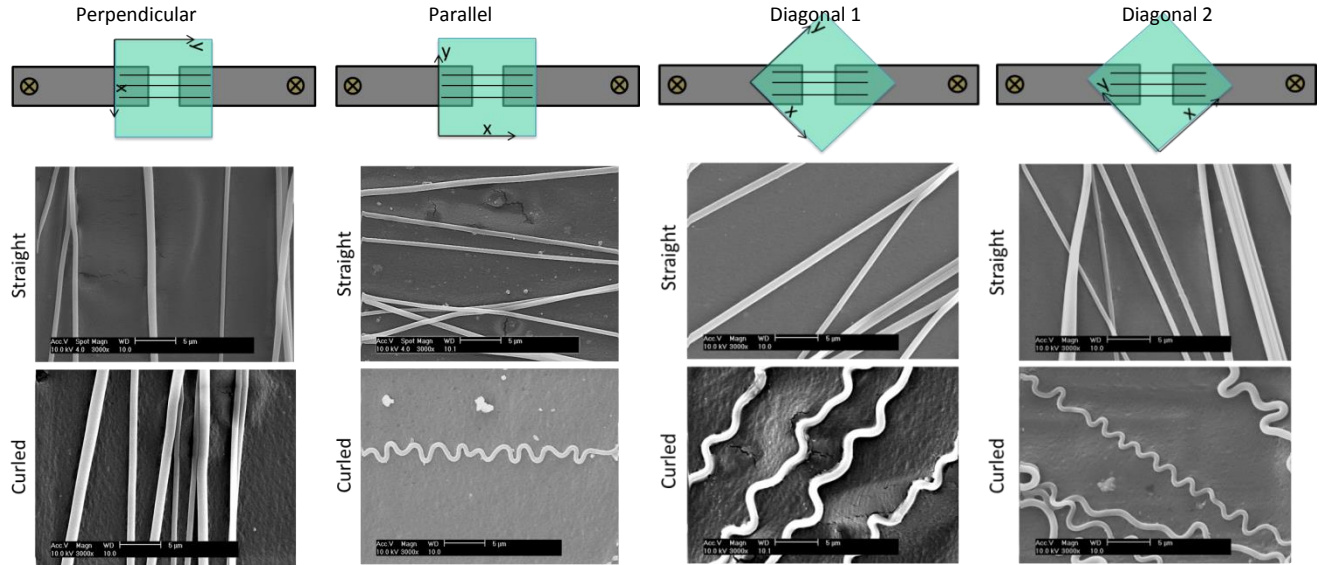


Figure 10 Comparison between the fibers deposited in different directions before and after shrinkage. Scale bars, 5μm.

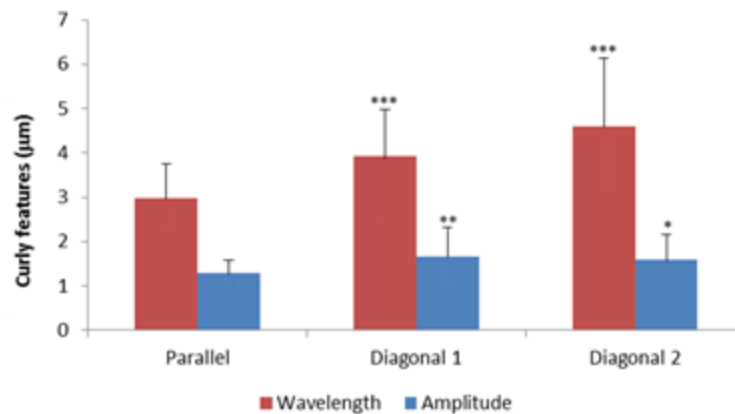


Figure 11 The wavelength and amplitude were measured for each configuration (parallel, diagonal 1 and diagonal 2) present in y-axis. The differences were statistically significant, ***p-value<0.001, **p-value<0.05 and *p-value<0.1.

The graph presented in figure 11 shows the wavelength and amplitude for each configuration of fiber deposition. The *parallel* configuration corresponds to deposit fibers along the shrinkage axis; the *diagonal 1* and *diagonal 2* corresponds to fiber deposition in a 45° angle (figure 10).

There are no measurements for vertical samples simply because when fibers are laid down perpendicular to the shrinking axis there are no curls, but just a compactness of the fibers. As it can be observed from the quantification the wavelength and the amplitude increased when the fibers assumed a diagonal orientation.

A comparison between *parallel* and *diagonal 1* configurations showed a significant difference ($2.97 \pm 0.76 \mu\text{m}$ vs $3.93 \pm 1.04 \mu\text{m}$, p-value < 0.001); when comparing fibers in *parallel* direction with *diagonal 2* the difference was also significant ($2.97 \pm 0.76 \mu\text{m}$ vs $4.59 \pm 1.54 \mu\text{m}$, p-value < 0.001). The difference between *diagonal 1* vs *diagonal 2* was also found significant $3.93 \pm 1.04 \mu\text{m}$ vs $4.59 \pm 1.54 \mu\text{m}$, p-value < 0.05).

For the amplitude the trend was the same: *parallel* vs *diagonal 1* was significantly different ($1.28 \pm 0.297 \mu\text{m}$ vs $1.67 \pm 0.66 \mu\text{m}$, p-value < 0.001), *parallel* vs *diagonal 2* was different but with a lower significance ($1.28 \pm 0.297 \mu\text{m}$ vs $1.59 \pm 0.57 \mu\text{m}$, p-value < 0.1). There was no significant difference between the two configurations of diagonal deposition.

4.4. Sacrificial fibers

Figure 12 shows the comparison between the scaffolds before and after immersion. The difference between them was visible, inclusively a partial loss of structure after immersion. The hopes were that the structure remained the same only with less fibers and more pores.

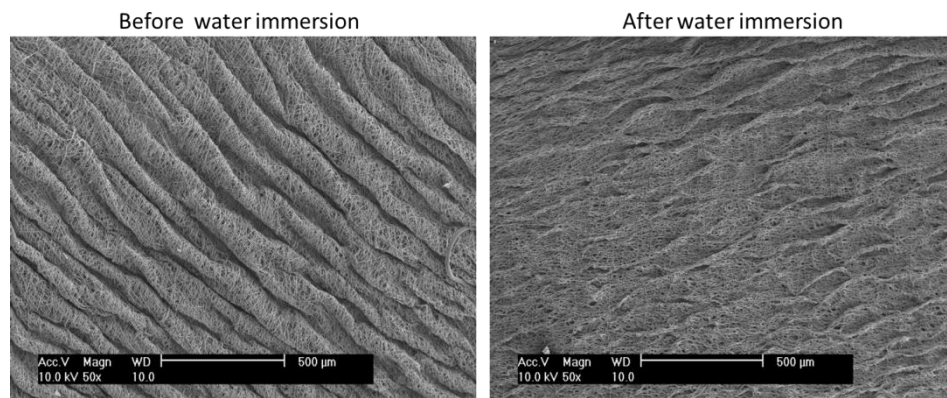


Figure 12 SEM pictures of PA-PVA simultaneously electrospun scaffolds before and after immersion in water and consequently removal of the PVA. Scale bars, 500μm.

The results from the experiments where the two polymers were electrospun in different orientations, and after shrinkage one was removed, are presented in figure 13. The removal of the

sacrificial polymer was distinguishable whether it was the first or second layer, despite the orientation. In figure 13 b, some curls seemed to have a different geometry. To assess if that was true the amplitude and wavelength were measured and the results are shown in the figure 14.

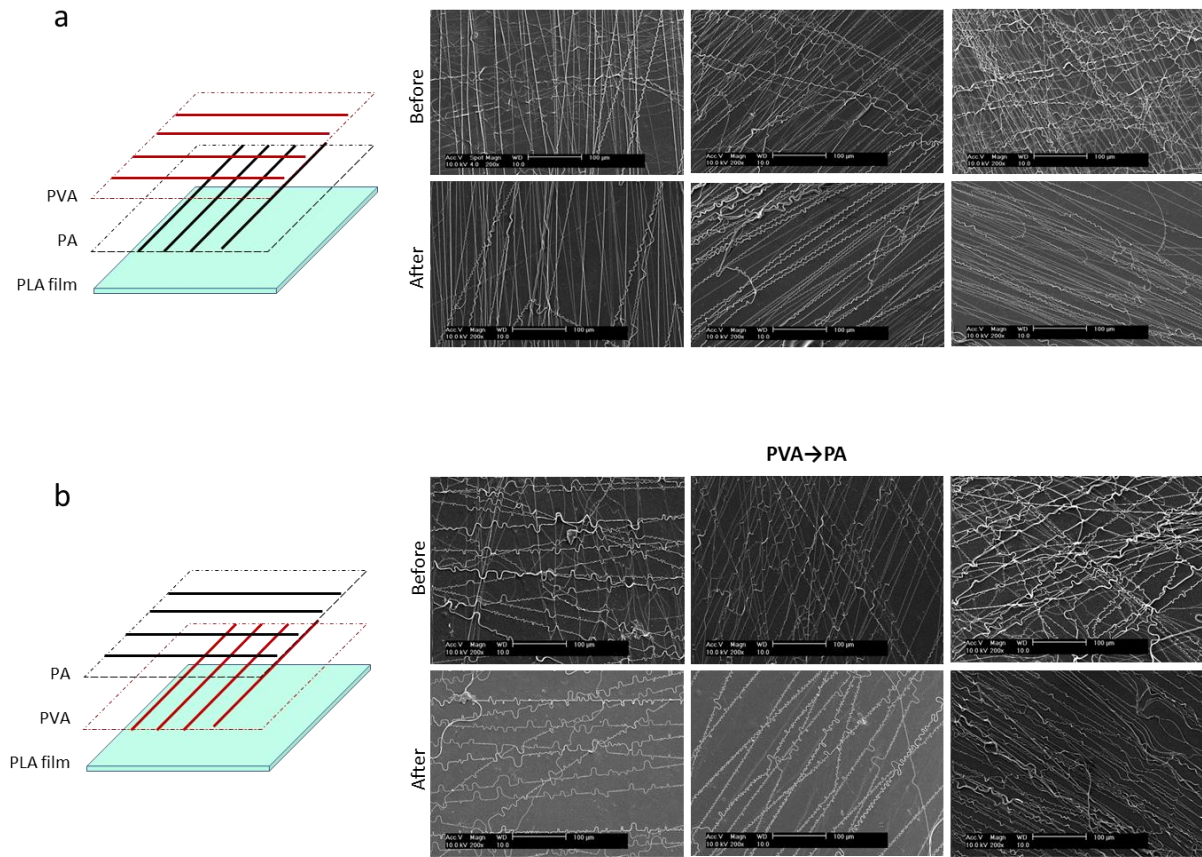


Figure 13 Removal of sacrificial fibers on low density scaffolds. The order of deposition was varied, in a) the first layer was PA and in b) the first layer was PVA as it is explained in the schematics. The SEM pictures show before and after immersion and consequently removal of the PVA. Some differences are visible in the crimp pattern. Scale bars, 100μm.

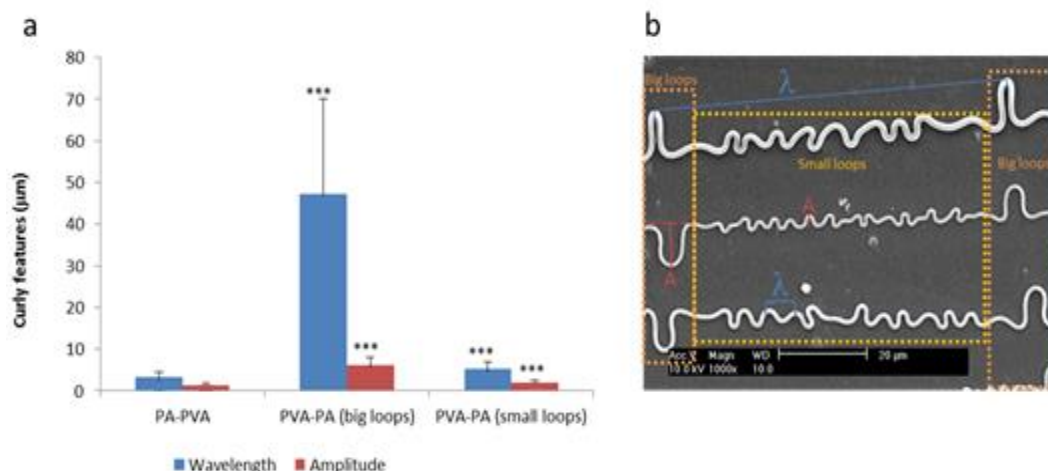


Figure 14 The graph in a) shows wavelengths and amplitudes measured (y-axis). The data was divided into 3 categories: PA-PVA which corresponds to PA as first layer of deposition and PVA as second layer and PVA-PA which corresponds to PVA as first layer and PA as second layer, p-value<0.001. The distinction between big loops and small loops is explained in the b) figure, where the same fiber has two different curls that were measured in separately. In b) is also described how the parameters were measured. Scale bar, 20 μm .

As it is possible to see in figure 14 a, three categories were made: PA-PVA, PVA-PA big loops and PVA-PA small loops and measured the wavelength and amplitude (y-axis). This distinction was performed, as it was possible to systematically observe the formation of bigger loops at periodical distances within the same fiber. The wavelength for PA-PVA samples was $3.24 \pm 1.32 \mu\text{m}$ whereas for PVA-PA the wavelength was $47.2 \pm 22.9 \mu\text{m}$ in bigger loops and $5.23 \pm 1.62 \mu\text{m}$ in smaller loops. The amplitude was $1.37 \pm 0.51 \mu\text{m}$, $6.20 \pm 1.83 \mu\text{m}$ and $1.92 \pm 0.51 \mu\text{m}$ for PA-PVA, PVA-PA big loops, PVA-PA small loops respectively. When the values were compared with the PA-PVA, the difference was statistically significant with a ***p-value < 0.01. These results indicate that by using this approach of including sacrificial fibers, it is possible to modulate the wavelength and amplitude of curls.

4.5. From single fiber curls to multiscale waves

As it was mentioned before, with the same process it is possible to have two different effects on the shrunk scaffold – curls or waves. The distinction between the two effects lied on the thickness of the fibrous mesh. Additionally, the thickness of the scaffold depended on the time of spinning; more time corresponded to a thicker layer of polymer and vice-versa. This experiment was designed to understand the threshold between the two effects and relate it to the thickness of the scaffold and to the time of spinning. Using a set of different times of spinning, several samples were produced, measured before shrinkage. Next these values were correlated with the structural conformation obtained (figure 15).

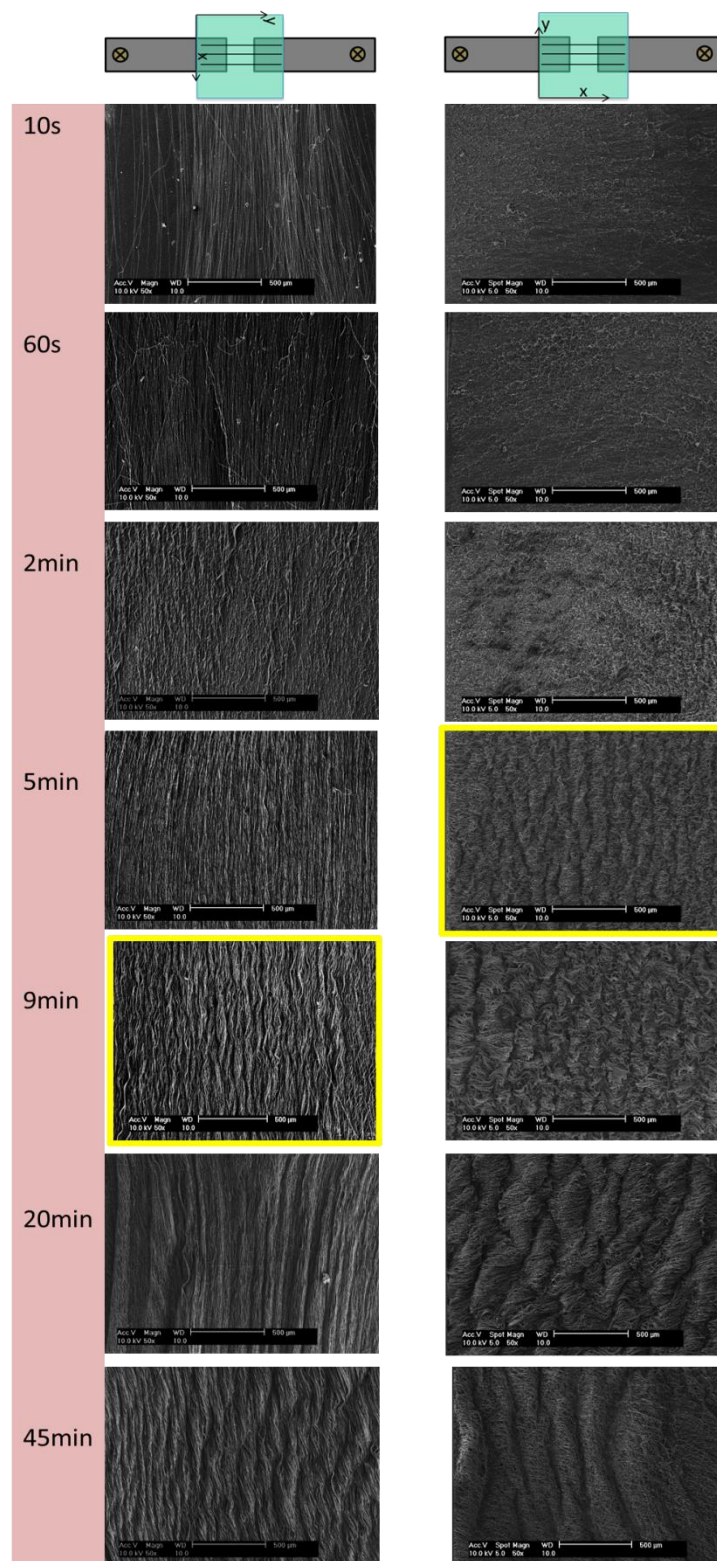


Figure 15 Topographical evolution as the time of deposition increased. The samples where fibers were deposited perpendicular to the axis started to show waves rather than only curls after 9 minutes of deposition whereas the perpendicular samples showed waviness after 5 minutes. Scale bars, 500μm.

For each time point, four samples were measured with a pair of calipers (*Mitutoyo America*) to assess the average thickness. For the wavy samples the global thickness was measured on top of the wave and the thickness of the film was discounted.

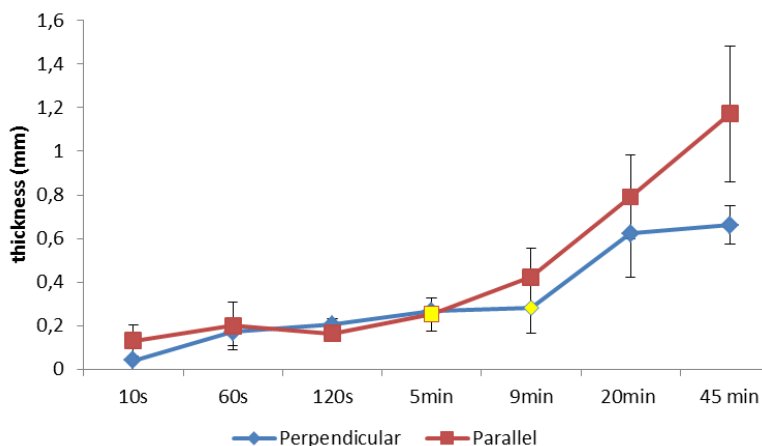


Figure 16 A graph depicting the thickness of samples with fibers deposited perpendicular or parallel to the shrinkage axis, according to time of deposition. In yellow is marked the transitional points from whether the scaffold more than curls evidence waviness.

From the data presented above in figure 16 and correlating that to the SEM images (figure15), it was possible to visualize that the wavy pattern started for the perpendicular samples at 9 min with an average thickness of 0.282 ± 0.116 mm, whilst for the parallel samples it occurred at 5 min with an average thickness of 0.252 ± 0.076 mm. Comparing these two values there was no significant difference between them and it was acceptable to admit that the waviness starts at thicknesses over 0.25 mm. This information allowed a more accurate selection of the desired pattern on the scaffold.

4.6. Different types of structures

Based on the thermal shrinkage of fibrous electrospun mats it is possible to have different structures only adjusting a few parameters, as it was already presented. The diagram below, figure 17, showed the possibilities explored. From 2D to 3D, from regular patterns to gradients, simple changes had a great impact in the final product.

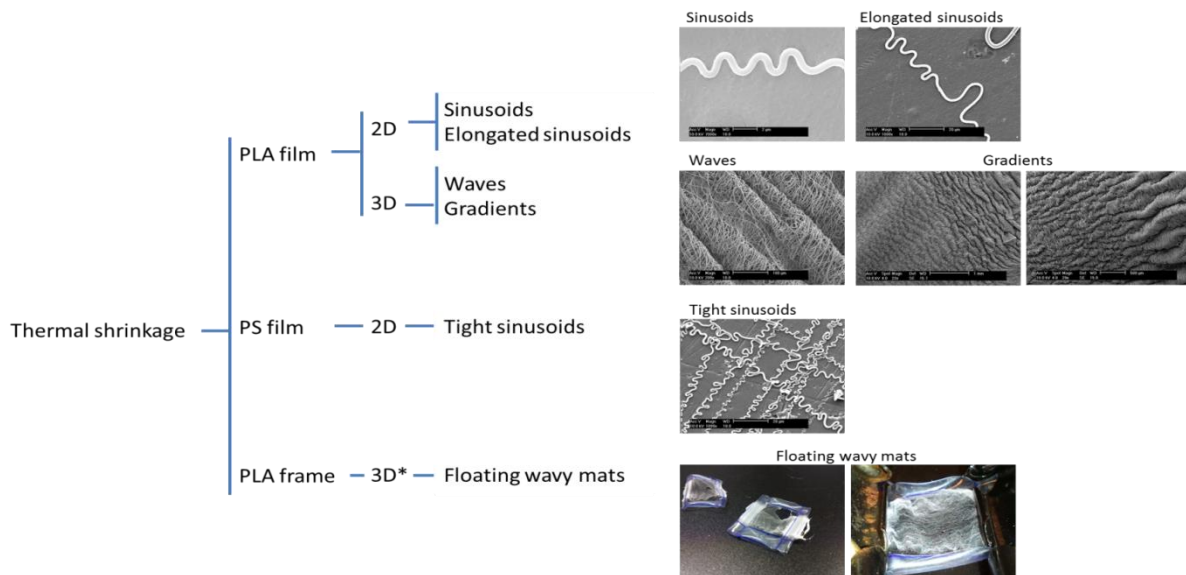


Figure 17 Diagram showing the possibilities created with these scaffolds and the thermal shrinkage based on the type of film used.

The wavy surface can assume a more regular pattern or a gradient depending on the proximity to the borders of the film. The region of the film closer to the electrodes (when they are mounted one on top of each other) exhibited a faded pattern because during the electrospinning the polymer is deposited on the film but there is always a portion that goes beyond the film and end up stuck to the electrodes. When the scaffold was removed from the electrospinning chamber, the mesh had to be carefully cut away from the electrodes (figure 18)

Assuming that the excess piece was preserved (figure 18 b), when the scaffold shrunk that piece remained flat because it did not have film underneath. Hence, a gradient was formed on the topography of the scaffold. The control of the gradient was not fully studied; its existence is known, but not the extension of it.

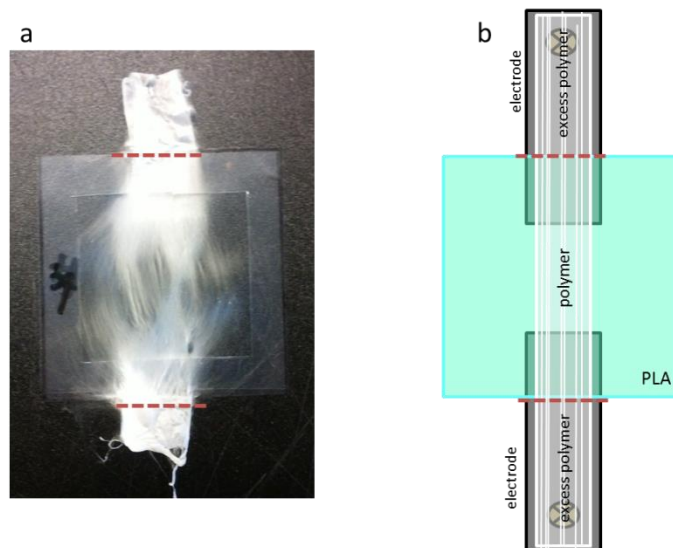


Figure 18 a) and b) Shows the extra polymer found when the scaffolds are free from the electrodes that can influence the shrinkage pattern of the scaffold.

The floating wavy mats fabricated on top of a PLA film were also checked under SEM (figure 18). Likely due to the weight of the gold-sputter coating against the delicate structure of the polymer it was not possible to preserve and observe the waviness on the surface but only the curls at the fibre level.

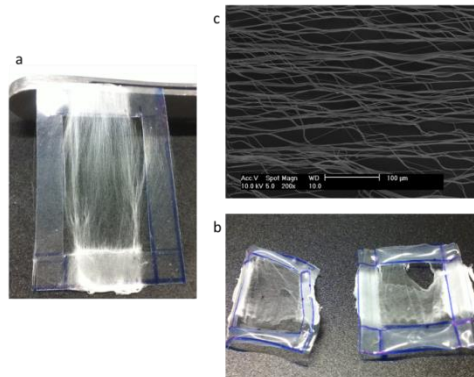


Figure 19 Figure a) shows an specimen of the floating wavy scaffold before and b) after shrinkage. In c) is showed a SEM picture of them. Scale bar, 100μm.

4.7. Pilot cell study

In this experiment hMSCs were seeded in three different substrates: PLA films free of PA fibers, wavy (high density) scaffolds of PA and the same scaffolds but flat. As this was a first trial with cells and these types of scaffolds, no parameter was quantified. The samples were stained with methylene blue and visualized under a stereomicroscope and under SEM.

The methylene blue assay enables the visualization of cells and their distribution across the surface. The cells are stained blue. Figure 20 depicts the three different substrates: PLA films, shrunk PA scaffolds and not-shrunk PA scaffolds. Cells were more spread on top of the PLA film (figure 20 a) when compared to the others, which may be possible because the surface is flat and cells created a spread monolayer. The scaffolds (figure 20 b and c) showed how cells were distributed at the surface level of a 3D structure.

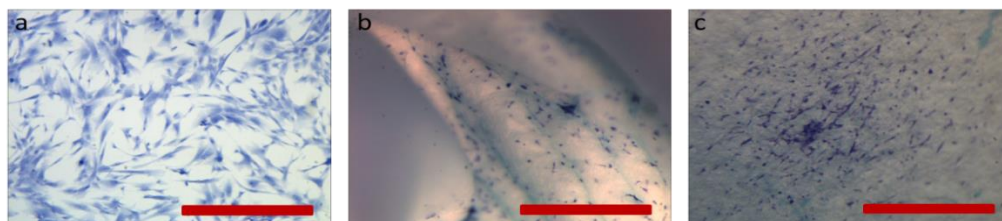


Figure 20 Methylene blue assay enables the visualization of cells and its distribution across the surface. a) corresponds to PLA film without fibers, b) corresponds to the shrunk PA scaffold and c) corresponds to not shrunk PA scaffold. Scale bars, 0.1 mm.

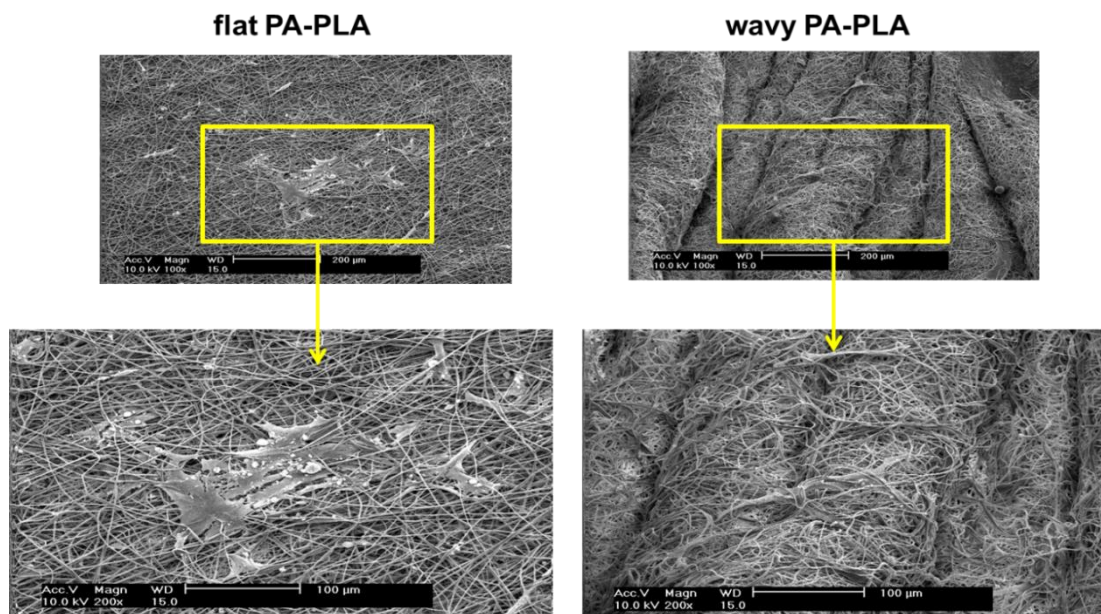


Figure 21 The SEM pictures shows cells on flat and wavy scaffolds and the differences found in their morphology. Flat scaffolds revealed spread and larger cells whereas wavy scaffolds showed more elongated and spindle-like cells. Scale bars, 200 μm and 100 μm .

Figure 21 shows two cellular populations found in this experiment. In general, on flat scaffolds, cells appeared more spread, occupying a larger area whilst wavy samples presented more elongated spindle-like cells.

Differences in the cellular shape related to periodicity and inherently curvature of the grooves were also found. Tighter waves (shorter periodicity) induced elongation. Looser waves (bigger periodicity) promoted cellular spreading (figures 22 and 23).

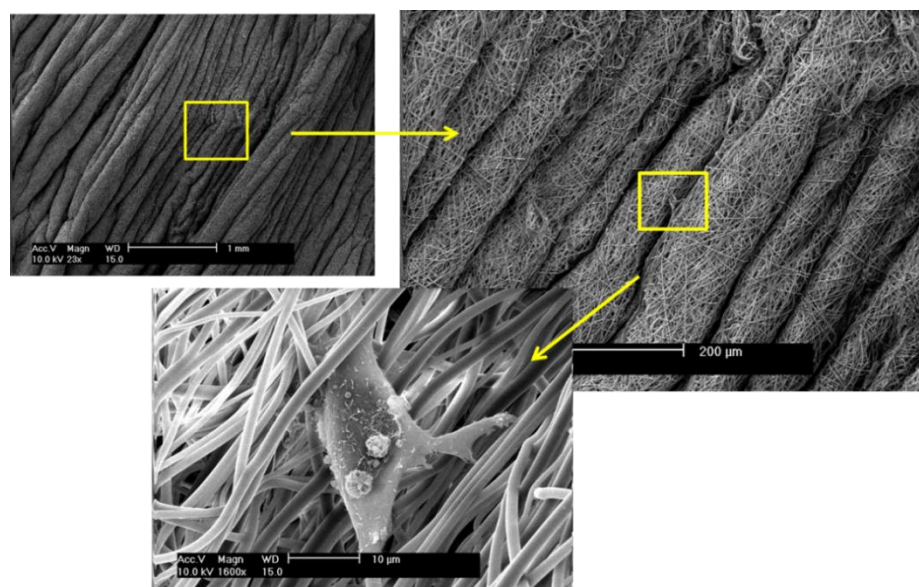


Figure 22 Series of SEM magnifications showing a cell on a tighter wavy scaffold bridging from one peak to the other. In these type of scaffolds cells tend to appear more elongated. Scale bars, 1mm, 200 μm and 10 μm , respectively.

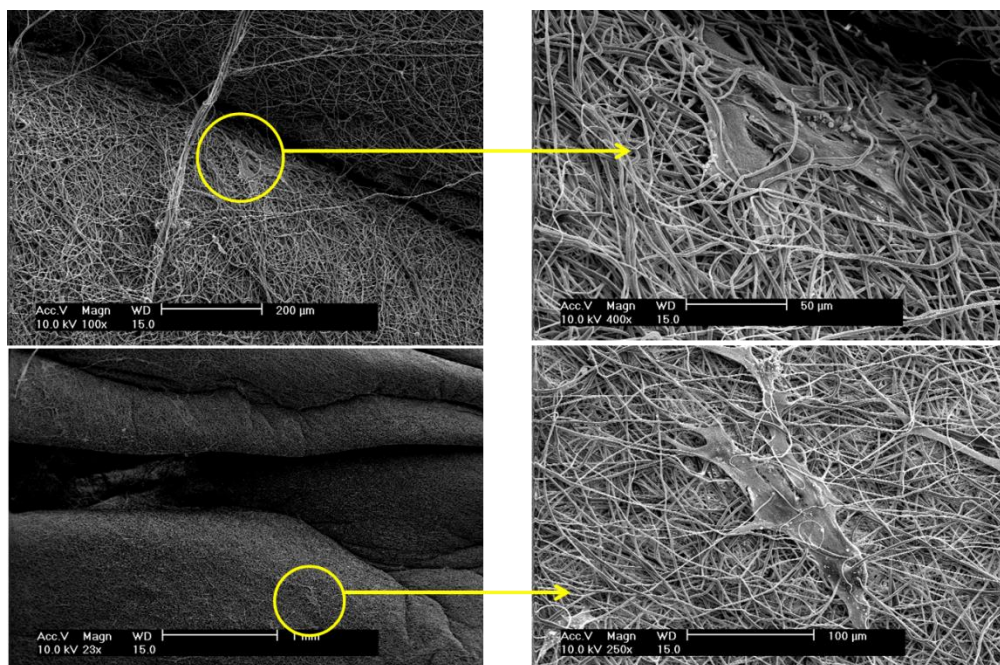


Figure 23 SEM magnifications of two examples where the looser waves tend to induce cell spreading. Scale bars, 200μm and 50 μm in the upper set and 1mm and 100 μm in the lower set of images.

A higher magnification revealed some cells entangled within the fibers. Figure 24 depicts four examples where cells were under the polymer web.

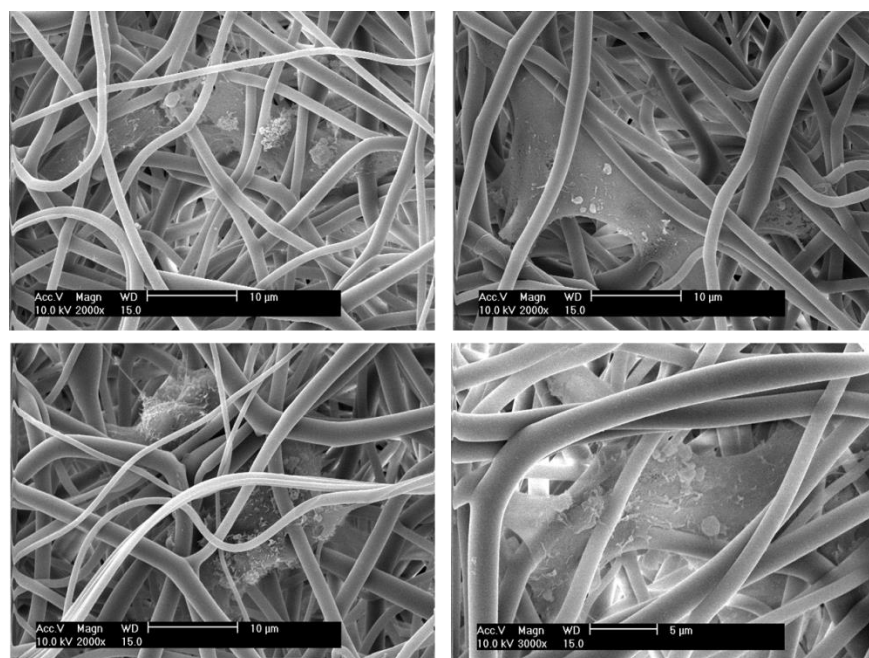


Figure 24 Cell entrapment in between electrospun fibers. Scale bars 10 μm and 5μm (bottom right).

4.8. Cellular ingrowth

Figure 25 represents the top view in flat and wavy samples, these pictures shows DAPI and Phalloidin labeling. As it can be observed from the pictures, Phalloidin staining was not successful as the labeling is not really specific.

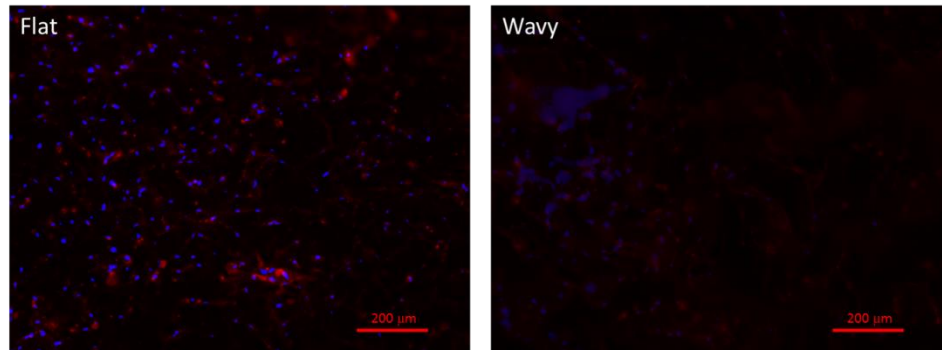


Figure 25 Dapi and Phalloidin merged images from top view in flat and wavy samples. Scale bars, 200 μm .

Figure 26 depicts four groups of images (bright field and DAPI) of different conditions according to the time point.

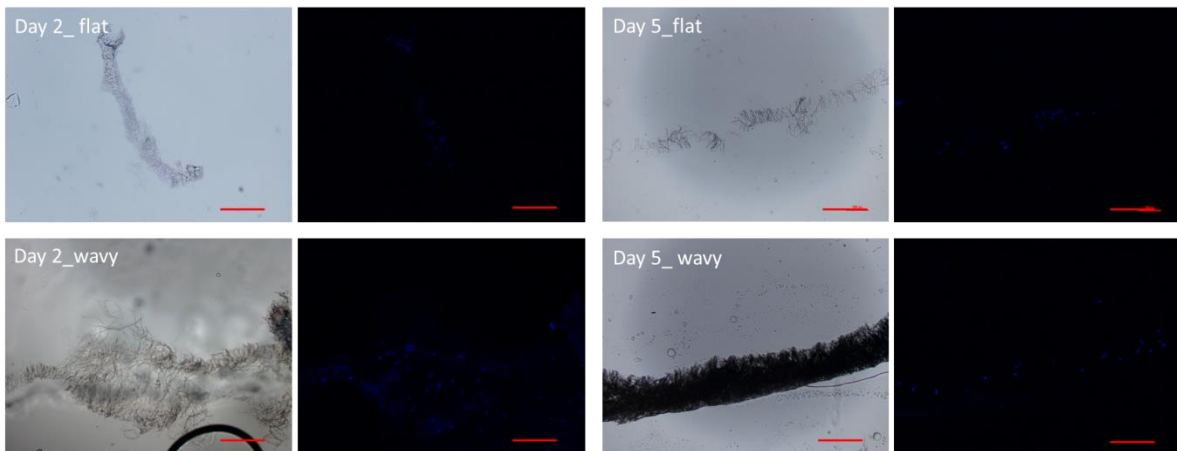


Figure 26 Bright field and DAPI images for two time points and respective conditions. The nuclei are labelled blue. Scale bars, 200 μm .

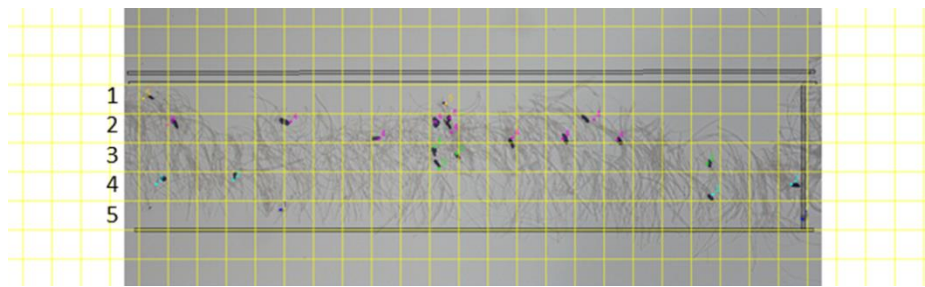


Figure 27 Grid created in ImageJ to measure cell infiltration along the cross-section. The numbers represent the bins, 1 corresponding to the top and 5 to the bottom.

Figure 27 shows the approach used to measure the number of cells in each bin in which the cross-section was divided. To facilitate the process the images were rotated towards their longitudinal direction. The outer bins (1 and 5) delimit and include the whole section. The first bin was considered the top of the scaffold and it was identified as the outer bin with more cells. Each bin corresponds to 3.6 ± 1.9 mm.

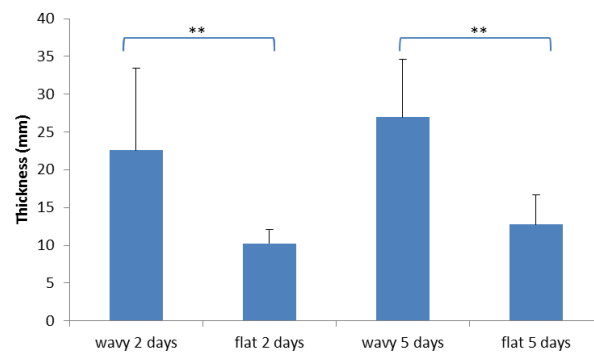


Figure 28 The graph shows the doubling effect in thickness registered after shrinkage. p-value <0.05

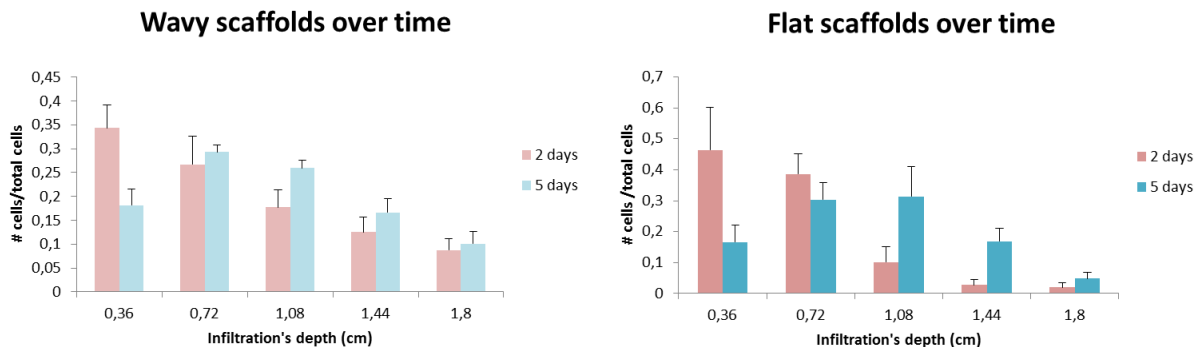


Figure 29 The two graphs represent the amount of cells present in each depth section of the scaffold. For each scaffold region, the number of cells was counted and normalized to the total cell number present in the sample and the thickness of the sample, therefore.

In order to confirm that wavy scaffolds were thicker than flat ones, the thickness was measured in 10 samples for each condition (figure 28). The difference between flat and wavy scaffolds is more than a two-fold (flat scaffolds: 1.2 ± 0.3 cm vs wavy scaffolds: 2.4 ± 1 cm). This is important when normalizing the number of cell in each bin as for flat scaffolds the bins are thinner than for wavy scaffolds.

Figure 29 shows the data from the cell counting. For each sample, cells were counted in each depth section. For each condition, 10 measurements were performed. To normalize the data the number of cells in each bin was divided by the total amount of cells in that cross-section. As not every sample has the same thickness not every cross-section has the same height, the depth presented in the x-axis corresponds to an average infiltration's depth. At day 2, cells displayed a descending distribution, the biggest amount of cells stayed at the top decreasing in number towards the bottom edge of the scaffold for both scaffolds. Despite presenting the same trend, flat scaffolds presented a higher concentration of cells on the upper region whereas wavy scaffolds showed a more even distribution (at 0.36 cm, wavy scaffolds: 0.34 ± 0.08 vs flat scaffolds: 0.46 ± 0.20 ; at 0.72 cm, wavy scaffolds: 0.26 ± 0.11 vs flat scaffolds: 0.38 ± 0.11). After 5 days of culture, cells were found at the bottom region in both scaffolds, thus, in wavy scaffolds, cells migrated up to 2.4 ± 1 cm compared to 1.2 ± 0.3 cm achieved in flat scaffolds, which corresponds to a two-fold increase in migration depth.

Over time, with cellular ingrowth, the spatial distribution became more even in both cases. The number of cells in the top layers decreased, whereas for the middle and bottom layers this value increased (figure 29). However, since the beginning of the cell culture, wavy scaffolds showed a more even cellular distribution across the scaffold when compared to flat ones which led to a less amount of cells reaching the deepest region of the scaffold (wavy scaffolds: 0.10 ± 0.05 vs flat scaffolds: 0.049 ± 0.049).

These results seemed, thus, to indicate that wavy scaffolds supported a faster homogenous distribution of cells through their thickness and a faster cell migration than flat scaffolds

4.9. Tendon /Ligament similarities

This experiment was repeated 3 times, with slightly modifications in each one.

First Trial

In this experiment we cultured MLEC in 3 different scaffolds: flat (negative control), wavy with fibers deposited in a parallel fashion to the shrinkage axis (wavy h) and wavy with fibers deposited in a perpendicular to the shrinkage axis (wavy v) for 8 days with 3 time points: 2, 5 and 8 days.

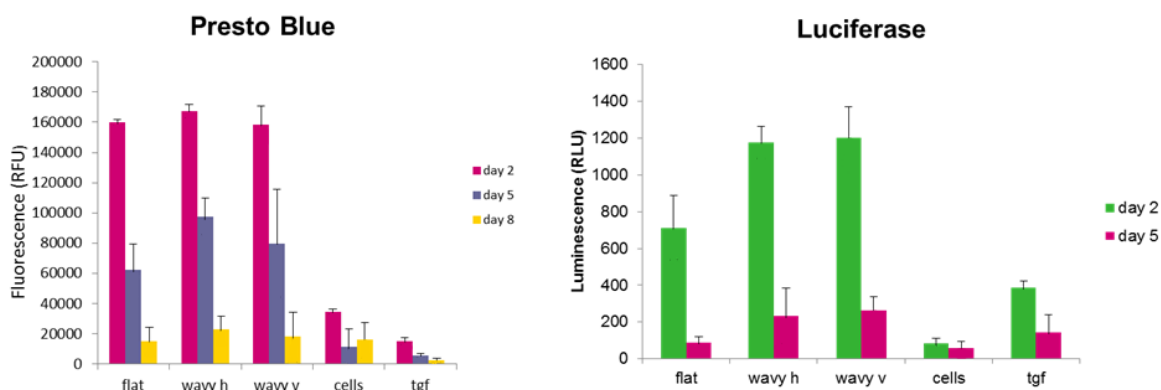


Figure 30 The Presto Blue graph shows the cell viability over time for each condition. The Luciferase data reveals the amount of light produced in each condition. Differences between *cells* and *tgf* samples when compared to others are due to differences in cell density

The results from the Presto Blue assay suggested a great difference between cell activity from MLEC seeded on scaffolds compared to MLEC seeded on TCP, which might be due to the difference in cell density (figure 30). In this trial the TCP was seeded with a cell density four times inferior to that of the scaffolds to avoid confluence as MLEC have a really quick proliferation. Despite this difference, it is possible to see that MLEC were working properly, as they proliferate less in the presence of the TGF- β 1 as it was expected. A comparison between the 3 scaffolds did not reveal any difference in terms of metabolic activity. Overtime, the metabolic activity decreased for all samples, indicating a possible decrease in viability, which could be explained by a lack of FBS in culture media.

The Luciferase assay results showed that cells responded as it was expected in the presence of TGF- β 1. When comparing the scaffolds, it was possible to see the difference between flat vs wavy regardless the orientation of the last ones (flat: 713 ± 176 RLU; wavy h: 1176 ± 88 RLU; wavy v: 1204 ± 165 RLU), with almost a two-fold increase in the signal in presence of the wavy patterns, thus suggesting a possible influence of such a multiscale scaffold topography on cell production of TGF- β 1. The tendency remained at day 5 (flat: 89 ± 29 RLU; wavy h: 233 ± 152 RLU; wavy v: 262 ± 75 RLU) (figure 30), though the luminescence values decreased in time.

Second trial

Based on these results, the experiments were repeated. In the second trial, the distinction between the two types of wavy scaffolds was discarded, as the difference was so small and the time points were modified to 2 and 3 days. The cell density is the same for every condition.

The second trial did not reveal the trend seen in the first. The difference, between the flat and the wavy scaffolds, was not significant neither for day 2 (flat: 4604 ± 1756 RLU vs wavy: 5276 ± 2168 RLU) nor for day 3 (flat: 1067 ± 201 RLU vs wavy: 1615 ± 447 RLU) (figure 31). The controls worked for both assays.

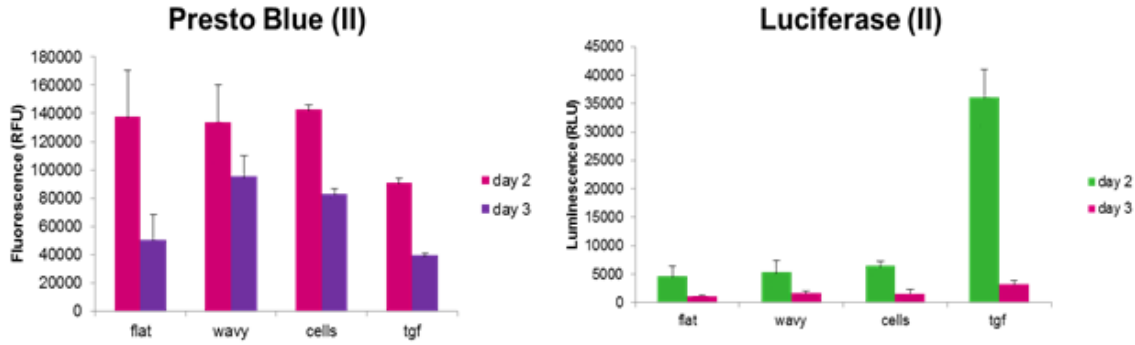


Figure 31 The Presto Blue graph shows the cell viability over time for each condition. The Luciferase data reveals the amount of light produced in each condition. Note that the results were not expected to be like this, the difference between flat and wavy samples is not significant.

Third trial

The experiment was performed a third time. In this experiment the TGF- β 1 control was substituted by 10% FBS, a cheaper alternative that does contain TGF- β in it as well. The wavy scaffolds were carefully chosen and it was only used one type of waviness (perpendicular) in order to be more consistent. The data was normalized with the DNA amount.

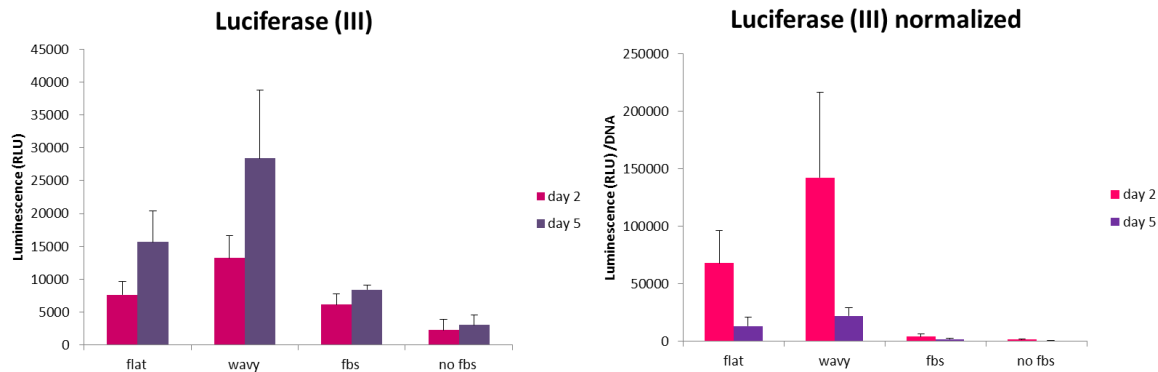


Figure 32 The graphs show the result for the Luciferase assay with and without DNA normalization for both time points.

The results of the third trial showed the trend found in the first trial (figure 32). Cells seeded on the wavy scaffold emitted more light than the cells seeded on the flat scaffold (figure 32). At day 2, the difference was significant with a p -value < 0.05 (flat: 7654 ± 1988 RLU vs wavy: 13248 ± 3349 RLU) whereas at day five despite the trend the difference was not significant with a p -value of 0.15 (flat: 15661 ± 4737 RLU vs wavy: 28381 ± 10367 RLU). The FBS control worked just as the TGF and showed that cells were behaving as it was expected.

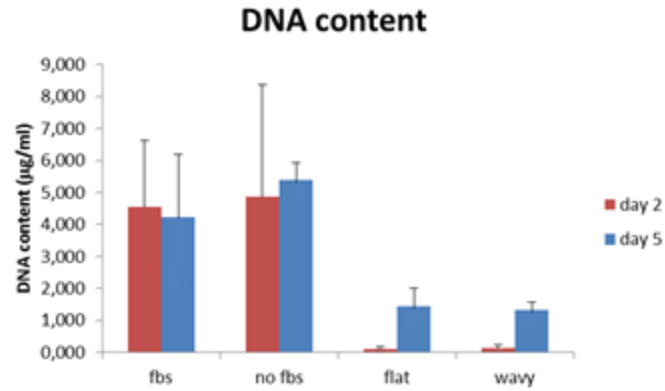


Figure 33 DNA content of the third trial of the tendon/ligament experiment.

The DNA assay allowed a data normalization and confirmed a decrease in cell content (figure 33). After normalization the same trend was present. Flat scaffolds induced less luciferase activity than wavy scaffolds at day 2, flat: 68097 ± 28113 RLU vs wavy: 142279 ± 74131 RLU; at day 5, flat: 13482 ± 7563 RLU vs wavy: 22237 ± 7422 RLU.

5. Discussion

The first part of the project allowed an understanding of the approach developed on curling fibres. Testing PLA's shrinkage ratios at different temperatures and times made possible to set 1 minute at 75° C as standard values (figure 6). The percentage of shrinkage chosen was around 60 %, which was enough to obtain the wavy effect. The maximum value registered was 67.5 % at 85° C, which resembles to the data given by the manufacturer (70 % at 85° C with 10 seconds exposure in water). This simple method ensures an easy and quick production of 2D curls which didn't have an impact on fibre diameter (figure 8 and 9). The initial diameter was 648 ± 308 nm. After shrinkage, this parameter remained constant with a value of 634 ± 259 nm.

Since the number of fibres remained constant, the final density of the construct (after shrinkage) depended on the initial density (before shrinkage), which increased as the sample decreased in size. This parameter could be adjusted by changing the temperature and time of shrinkage, influencing the shrinkage ratio.

The next section showed that the curly patterns can be modified by varying the orientation of the fibres relatively to the orientation of the PLA film (figure 10). The angle between the fiber and the shrinking axis had an impact on how the curls formed. When fibers were deposited in the same direction as the shrinking axis, the wavelength and amplitude were significantly lower compared to when fibers were deposited in a diagonal direction (*parallel* vs *diagonal* 1: 2.97 ± 0.76 μm vs 3.93 ± 1.04 μm and *parallel* vs *diagonal* 2: 2.97 ± 0.76 μm vs 4.59 ± 1.54 μm) (figure 11). When fibers were deposited perpendicular to the shrinking axis no curling happened. This configuration only allowed fibre compactness, because as the film shrunk, the space between each fibre decreased, bringing the fibres closer.

The curl shape can also be changed with changes in fiber deposition. For the *parallel* samples, curls resembled a sinusoid while in the diagonal samples curls assumed a more triangular shape or displayed a slight tilting (figure 10). This analysis did not take in to consideration possible changes in fiber diameter which might influence the fiber curling and the underlying wavelengths and amplitudes.

In order to create more free volume, the selective removal of certain fibers was studied. Thicker electrospun mats (~1mm) were made of PA and PVA (water soluble polymer) blends. The expected result of having single curled fibers was surpassed by the creation of a topographical pattern. Upon shrinkage, the mat puckered forming a well-defined crimple effect. After the water immersion/emersion, the pattern slightly faded out and the structure seemed not totally preserved (figure 12). The dimensional instability of the constructs, after removal, was also referred in the previous work of *Baker et al.* where they found that above a certain threshold of sacrificial fiber removal, cell infiltration was improved indeed, but the remaining fibers weren't

robust enough to endure stress and retain the structure. Conversely to their work, the scaffolds in this study did not experienced shape distortions.

Regarding the free volume inside the scaffold, the voids that were created during shrinkage, possibly decreased in number or volume with the structure collapsing. Hence, the ultimate goal of this experiment (to improve cell infiltration) has to be tested with a proper cell study. A cross-section analysis would complement and support this information. A possible explanation for the partial collapse could be that the failure of the structure might be due not to the PVA removal but to the immersion/emersion and the surface tension experienced when the scaffold is removed from the water-bath. Further experiments should be performed to explore this possibility.

Thinner mats of PA-PVA were fabricated in different configurations and the PVA was removed afterwards through water solubilisation. The sequence of deposition was revealed as an important aspect, since it may dictate the type of curls created. From figure 13, the differences between the fibers when PVA was the first or the second layer could be observed. The conformation of the PA fiber depends on whether it stays under or on top of the PVA. If the PA was the first to be electrospun and it stood under the PVA, it acted as a “bed” for the fibers on top, but once they were removed there are no changes; on the other hand, when the opposite happened the PVA supported the PA and this adapted itself to what was under, meaning the PVA mesh. In this way the PA was molded by the PVA and assumed a different conformation. After the removal of the PVA, the PA curls collapsed and the 3D structure became a 2D curl with bigger amplitude, maybe due to lack of support or due to the transition from the water-bath to air drying.

So far, selective fiber removal had never been used for the creation and manipulation of fiber shape. As figure 14 depicts, the shape of the curl changes with the order according to which the polymers are deposited. Some measurements were performed and the wavelength and the amplitude were compared between the two configurations (PA first and then PVA and the reverse). Generally, the samples with the PA as a first layer had a shorter wavelength ($3.24\text{ }\mu\text{m} \pm 1.32\text{ }\mu\text{m}$) and smaller amplitude ($1.37\text{ }\mu\text{m} \pm 0.51\text{ }\mu\text{m}$).

For the PVA-PA samples, meaning first layer being PVA, the curls exhibit a binary populations of loops. The big loops correspond to the site where the PVA was before removal and the smaller correspond to fibers that were always in contact with the PLA film (figure 14). A significant difference in amplitude could be observed when comparing small and big loops, being $1.92\text{ }\mu\text{m} \pm 0.514$ vs $6.21\text{ }\mu\text{m} \pm 1.83\text{ }\mu\text{m}$, respectively. The difference in the wavelength between the two different groups was also significant, and despite the variability there was a twenty fold ($5.23\text{ }\mu\text{m} \pm 1.62\text{ }\mu\text{m}$ vs $47.2\text{ }\mu\text{m} \pm 22.9\text{ }\mu\text{m}$) increase in wavelength for the big loop fiber population.

Therefore, changing simple parameters (time of spinning) or even using a different type of film (material or shape) results in different scaffolds. The curls can be modified by changing the direction of deposition, including or not a sacrificial polymer and depending on the film chosen.

The observation that the morphological effect produced was strongly correlated to the thickness of the fibrous mat arose the necessity of further investigating how these scaffolds

behaved. The changing point from curly fibres to wavy mat was studied (figure 15). Depending on the orientation of the fibers, it could be at an average thickness of 0.282 ± 0.116 mm (perpendicular samples) or of 0.252 ± 0.076 mm (parallel samples) (figure 16). These thicknesses were related to the time of deposition. For perpendicular samples after 9 minutes of electrospinning, the thickness was enough to originate a wavy pattern. Parallel samples needed only 5 minutes to achieve the effect. There was no significant difference between them and it was acceptable to admit that the waviness occurs for scaffolds with thicknesses over 0.25 mm.

The fabricated scaffolds can assume different structural configurations, which is promising as it may mimic the native tissues which are organized by hierarchical levels (from the nano up to the macroscale). From the microscopic level (curls) to macroscopic level (waves), the scaffold assumed different hierarchies of spatial organization. The floating wavy mats were created thinking about the possibility of reducing the influence of the film under the polymer, as it may influence cellular sensing. These levels are cumulative meaning that the highest level of organization also contains the lowest. Although the most notorious feature of the 3D scaffold is the wavy pattern, the curling at fibre level is still present but it is merely masked by another effect. Therefore, even if the waviness was lost, the curling effect remained.

Previous methods used to curl electrospun fibers showed similar results to the ones achieved in this project, but with a narrow range of wavelength. *R. Kessick and G. Tepper* produced 2D helical structures with diameters that ranged around $2 \mu\text{m}$ which were much thicker than the ones fabricated in this study. Changing the PEO content of their composite, they could modulate the curling of the fibers. Thus, for higher PEO contents the wavelength appeared to decrease and the helical fiber seemed more compact. From one of their SEM analysis is possible to see structures with a wavelength around $5 \mu\text{m}$ which is in the range from the ones produced (from $3.24 \pm 1.32 \mu\text{m}$ up to $47.2 \pm 22.9 \mu\text{m}$). Trough inclusion of a harmonic movement during electrospinning, *Bin-Sun et al.*, created 2D curls with wavelengths around $5 \mu\text{m}$. they stated that increasing the rotating speed, the alignment of the curly fibers was improved. They did not explore the modulation of the curl shape nor analyzed parameters as the wavelength and amplitude. Based on a complex method of calcination and reduction of copper, *Guoqing Chang et al.* produced 3D helical ribbons. Their fibers presented a diameter of $2.6 \mu\text{m}$ and a wavelength of $3.2 \mu\text{m}$. Cheng-Chan Tang et al., using a nail tip collector fabricated 3D curly fibers with 100 mm of wavelength. In this study a simple method is presented that enables a big variety of outcomes in terms of curl shape and dimensions.

Using a lower cell density, different scaffolds were seeded and observed at day 28. Through this period, cells were able to sense and readjust themselves to the new environment assuming different characteristics. The results showed primarily two populations of hMSCs. This distinction was made based on their morphology. As it is possible to see in figure 21, some hMSCs were more spread and circular than others which were more elongated and spindle-like.

The disparity in cell shape could be assumed as a consequence of the impact that the scaffold has on the cells seeded. Comparing the wavy and flat scaffolds, a correlation between the

periodicity of the pattern and the cell shape was found. When the grooves were larger (bigger periodicity), the distance between two peaks was big enough to prevent cells from bridging across two peaks. Conversely, if the distance between two peaks was small (around 100 μm), cells started to elongate and even traverse from one groove to the next (figure 23).

The explanation for this duality may lie on the extension of the focal adhesions and the area available for that. The large grooves had small curvatures, which mean that they were more exposed to cells to adhere to, while the opposite happened for thin grooves.

A certain degree of cellular migration towards the bulk of the scaffold could be also observed. Despite not being the best approach to confirm this infiltration, SEM analysis is an initial proof that there are cells inside the scaffold, which is beneficial considering that the one drawback of using electrospun scaffolds in tissue engineering is the poor cellular ingrowth.

Speculating about the morphologies found in these samples, the observations may point out to a differentiation maybe into an osteogenic lineage (due to a spread morphology)³⁷ or even myogenic lineage (due to spindle-like shape)⁴⁰, but the lack of information about focal adhesions and about specific differentiation markers prevents a further accurate discussion. The low cell density used in this experiment may have also influenced the cellular commitment as it is known that with low densities osteogenesis is predominant, while with high cellular densities it is possible to achieve chondrogenesis and even adipogenesis^{36,38}. Cell density is strongly bound to culture configuration and cell displacement during culture. If the cell density is increased, cells are really packed together and they establish more cell-cell bonds than cell-substrate bonds (focal adhesions)³⁶.

As the scaffolds shrunk, their thickness increased, more precisely doubled in size (flat scaffolds: 1.2 ± 0.3 cm vs wavy scaffolds: 2.4 ± 1 cm). The doubling effect in thickness is important to take into account. As the scaffold thickens, cells tend to have more difficulties to migrate towards the central region.

After 5 days of culture, cells were found at the bottom region in both scaffolds, thus, in wavy scaffolds, cells migrated 2.4 ± 1 cm compared to 1.2 ± 0.3 cm achieved in flat scaffolds (figure 29 and 30).

Comparing these results with previous studies, the depth of cellular penetration registered was considerable higher in this case. *Vaquette et al.*, started with 700 μm thick patterned scaffolds and, at day 7, cellular infiltration reached up to 250 μm , while in random scaffolds, cells only migrated 50 μm ¹⁹. Making use of the salt leaching technique, *Nam et al.*, achieved cellular migration up to 3.5 mm in 5 mm thick scaffolds²⁵. *Baker et al.* fabricated scaffolds with increased porosity using the selective removal of sacrificial fibers where cells migrated 0.5 mm at maximum over three weeks⁵³.

In these previous works mentioned, the analysis was based on the maximum distance that cells migrated. The number of cells through the scaffold was not discussed. In this case, as both

scaffolds allowed complete penetration (at least for some cells) is necessary to assess how many cells migrate into each region of the scaffold and then compare between scaffolds.

Our results showed that at the first time point, day 2, the majority of cells were at the top which was expected¹⁹. Over time, the cell number decreased at the top of the scaffold whereas in the middle and bottom regions, the cell number increased, suggesting cellular ingrowth (figure 29).

Regarding spatial distribution, wavy scaffolds demonstrated to have a more even cell distribution along the cross-section than flat scaffolds (figure 28). Since day 2, wavy scaffolds had a more even cell number across the sample thickness, whilst flat scaffolds had a higher cellular concentration on the upper regions and few at the bottom. Despite the similar distribution at day 5, the results may support the hypothesis that wavy scaffolds enable a faster and more homogenous cellular ingrowth.

In this sense, wavy scaffolds enabled a more even cellular ingrowth than flat scaffolds. Finding a way to assess porosity would be advantageous to consolidate on whether this novel scaffold could substantially improve cellular infiltration and become an asset in tissue engineering.

Assuming some resemblances between the high density wavy scaffolds and natural tendon/ligament, it was formulated the hypothesis that the scaffold topography could mimic the organization of collagen fibers in tendons, this affecting TGF- β production.

Using a MLEC line, it was possible to assess this information, due to its modification with a promoter known to respond to TGF- β production by light emission via luciferin-luciferase transformation⁵². Hence an increase in the luciferase activity corresponds to an increase on TGF- β signaling.

The results from the first trial showed that the scaffold's waviness resulted in a difference in luciferase activity, with cells seeded on flat scaffold emitting less light than cells seeded on wavy scaffolds. Relating the amount of light produced with TGF- β signaling, it seems that wavy scaffolds mimicked its presence and that is translated in more emission of light. This effect was seen over 5 days (figure 30).

In the second trial, the results went not significant, despite the same trend (figure 31). One of the reasons that may explain the failure of this trial could be the heterogeneous selection of wavy scaffolds. Based on the idea that the differences between the wavy v and wavy h scaffolds were so small, both were, incorrectly, included.

The third trial combined the luciferase assay with the DNA assay, enabling a normalization of the data based on the cell number. These results corroborated the first trial exhibiting that the wavy scaffolds induced TGF signaling over the flat ones (figure 32). The decrease in cell number over time may be due to the lack in FBS in the culture medium which was not included to

preventing any misunderstandings or masking effect on the results because it already contain or should contains TGF.

It was already shown, that a grooved silica substrata, with 5 μm depth, can induce and improve the healing of completely divided rat flexor tendons *in vitro*⁵⁴. The scaffold used in our study is around 1mm thick, thus the depth of the grooves is higher than the 5 μm tested in the previous mentioned work. To further investigate if the effect on tendon healing is similar, it would be necessary to run a qPCR to identify at the gene level if primary cells or hMSCs are differentiating into tendon/ligament cells when seeded on wavy scaffolds. Further studies should be also conducted to proof that our findings *in vitro* can be also correlated to functional regeneration *in vivo*. Nevertheless, in this study we have showed that it is viable to use electrospun scaffolds without the concerning about the lack in cellular infiltration and moreover, that through thermal shrinkage it is possible to create a topographical pattern that increases the TGF- β production.

6. Similarities between native tissues and the multiscale scaffold

Looking up at the bibliography for pictures of curled/wavy natural structures, a few native tissues, beyond the known tendon and ligament, were discovered as having these crimp patterns. The follow set of images shows a few examples that with some adjustments could be recreated with the multiscale scaffold here proposed.

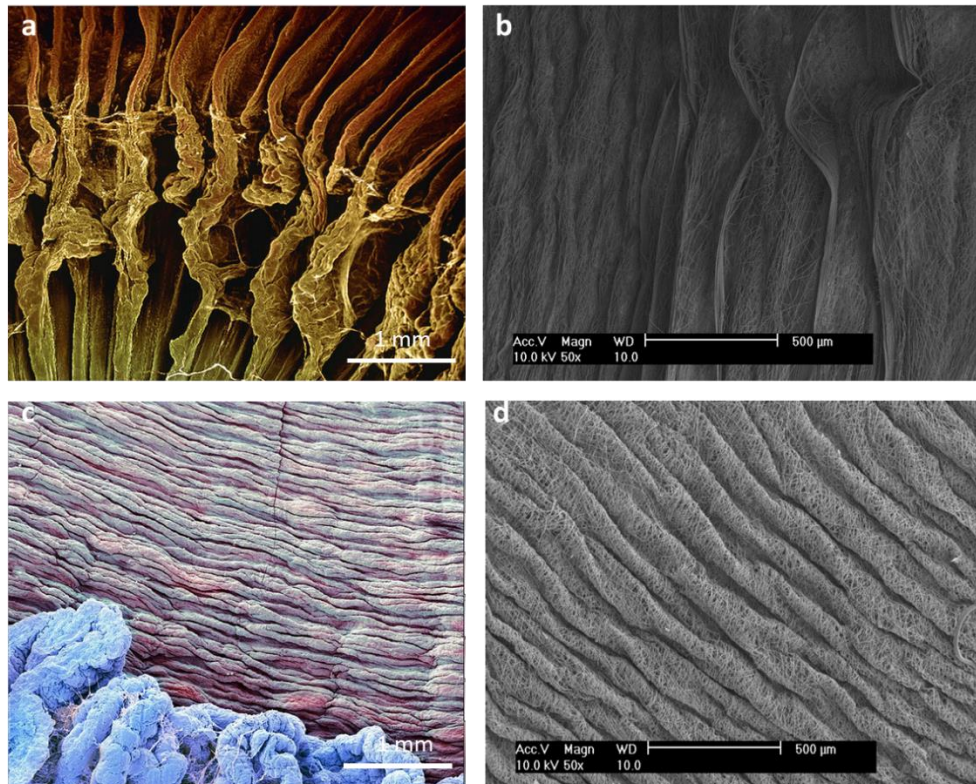


Figure 34 Figure a) show a SEM image of a ciliary body and c) a SEM image of the iris (scale bars, 1 mm; from www.sciencephoto.com), compared to b) and d) SEM pictures of two different configurations of the multiscale scaffold.

The figure above, shows two SEM pictures of the ciliary body (figure 34 a) and the the iris (figure 34 c), both part of the human eye, and some SEM pictures of the multiscale scaffold, showing the possible resemblance between the topography obtained and the native tissue.

Figure 35, shows an artery wall composed of curled collagen fibers interconnect by a matrix, whose configuration is quite similar to a low density shrunk scaffold.

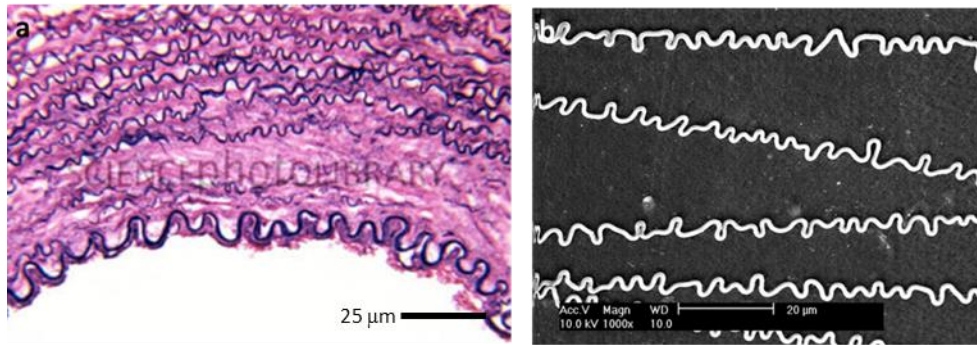


Figure 35 Figure a) shows artery wall composed by curled elastin bundles separated by collagen (scale bar, 25 μm) compared (from www.sciencephoto.com) to b) a shrunk low density scaffold with curly fibers (scale bar, 20 μm).

The trachea (figure 36) also displays a crimp pattern that could be mimicked by a high density wavy scaffold that was electrospun for 45 minutes with fibers lying down perpendicular to the shrinkage axis.

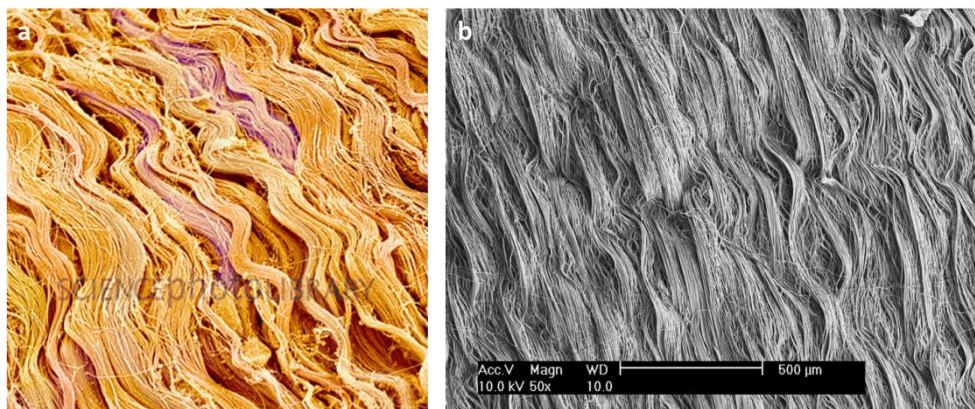


Figure 36 SEM image of tracheal wall displaying a crimp pattern (from www.sciencephoto.com) compared to one of the forms of a high density shrunk scaffold.

Despite not knowing the scales, these examples serve as incentives to further explored and optimize the multiscale scaffold developed in this project as it may serve different clinical applications.

7. Conclusions and future work

This thesis discusses and investigates a novel approach on tailoring crimp patterns on electrospun fibers by using thermal shrinkage.

The method here developed and applied stands out from others described, because of its simplicity. Instead of using complex setups or chemical treatments, it is based on thermal shrinkage of a polymer film that serves as a vehicle to induce the crimping effect. As the PLA film shrunk the PA electrospun fibers, which were deposited on top, adjusted their conformation to the new dimensions of the film, becoming curly. The patterns created depended on a series of parameters such as: (i) the fiber density, which is related to the fiber diameter (not explored in this project) and time of electrospinning/deposition; (ii) orientation in which fibers are deposited relatively to the shrinkage axis, and (iii) the polymer film used (mono- or bi-oriented). The application of the selective removal of sacrificial fibers can also be used to create different configurations. Combining all these tools is possible to tune and adjust the multiscale system to each different clinical application.

As the scaffold by its own does not have a function, it was crucial to investigate how cells reacted to it. A pilot cell study was presented, where for the first time hMSCs had contact with this type of scaffold. The 28 days culture showed that cells were expanding in the scaffold and that some appeared to be differentiating. This assumption was made based on cell morphology via pictures taken under SEM. Two populations were identified: spread cells and elongated cells. According to literature, cell shape is intimately linked with differentiation. Some studies support the idea that cell shape is a consequence of differentiation but recently there has been an increasingly set of evidences that cell shape can be the cause of differentiation and not only a consequence³⁶. Hence, cells with a more spread and bigger area often express osteogenic genes whereas spindle-like cells express myogenic genes.

Cellular migration is also one of the major concerns that investigators face when using electrospun scaffolds in tissue engineering. The hypothesis was that if the crimp pattern increases the three-dimensionality and the free-volume inside the scaffold cell permeability is also increased, cells can migrate towards the bulk of the scaffold easily and evenly. The results showed, despite the great deviations, that wavy scaffolds enable a more even distribution of cells across the scaffold which is important in tissue engineering. Since day 2, the bottom part of the wavy scaffolds had a considerable amount of cells which did not happen with flat scaffolds. The transition from results to conclusions will only be possible if complemented with an analysis of scaffold porosity to ensure that there is also an increase in free-volume. Currently, there is evidence that cellular infiltration is better in wavy electrospun scaffolds than in flat electrospun scaffolds.

Impelled by the similarities between a high density wavy scaffold and native tendons/ligaments, an experiment was designed to evaluate if these scaffolds were able to

stimulate cells in the same fashion as TGF β . Therefore, a transfected cell line (MLEC), that had a PAI-1 promoter fused to firefly luciferase, was cultured on the wavy scaffolds. As it is known, TGF β stimulates PAI-1 expression, thus in the presence of TGF β the activation of this pathway would be increased and so the production of light. Applying this concept to the scaffold means that if the topography could induce differentiation towards a tendon/ligament cell line, the scaffold would mimic the presence of TGF β and stimulate the production of light. The experiment was repeated 3 times (two with success) and indicated that cells seeded on wavy scaffolds produced more light than cells seeded on flat scaffolds. All the presented evidences suggested that the wavy scaffolds can improve cellular migration and are promising candidates for tendon and ligament regeneration.

The consolidation of the results obtained is crucial in the future exploration of this multiscale scaffold. As it was mentioned there are a few possibilities to enrich this work that due to lack of time were left behind. The evaluation of scaffold porosity should be done in order to conclude if the curliness of fibers really increases the free-volume inside the scaffolds and from that decide if the cellular infiltration benefits from the increased three-dimensionality. A further study of cellular differentiation would be important to confirm if the topography is inducing differentiation and in this case towards which cell lineage in more depth details. The tendons/ligaments study could be explored using a cell population that has clinical relevance.

8. Attachments

A)

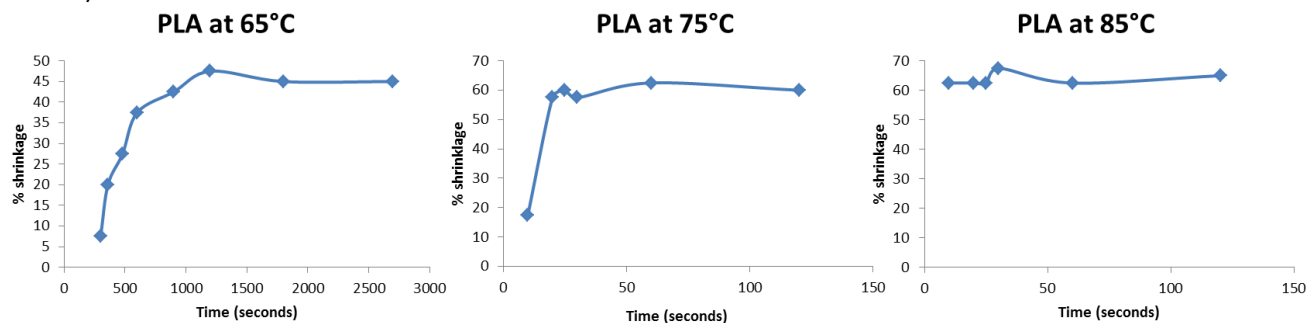


Figure A Shrinking properties of the PLA film at different temperatures over different times.

B)

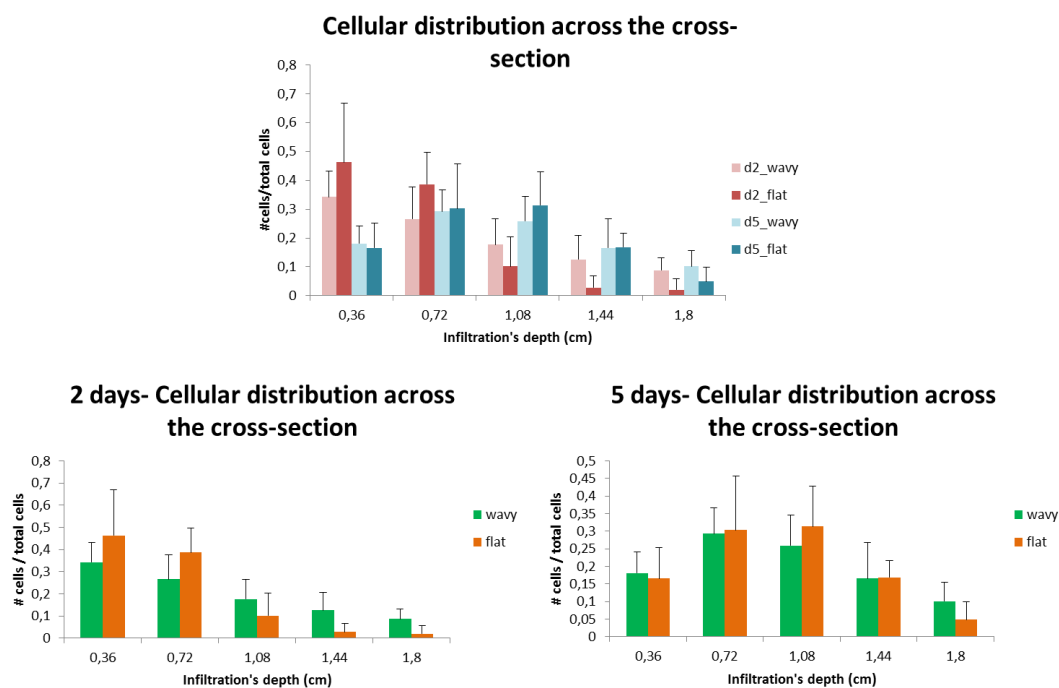


Figure B Cellular ingrowth data including cell distribution across the thickness of the scaffold and cell distribution for each time point.

c)

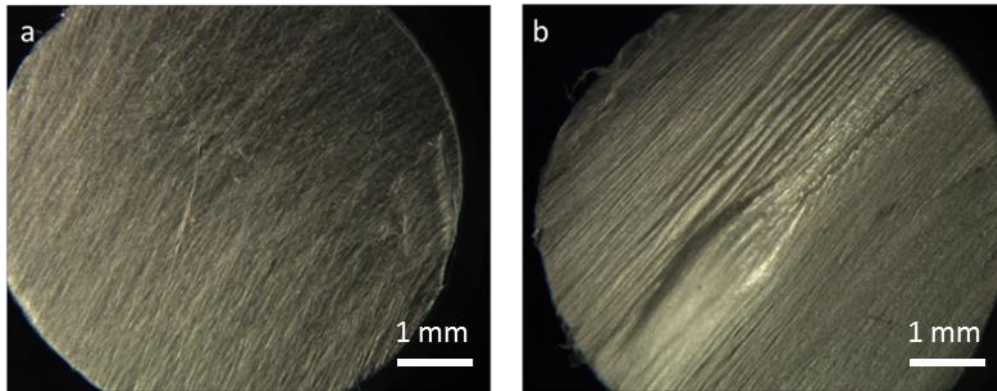


Figure C Stereomicroscopic images of a flat scaffold (a) and a wavy scaffold (b) used in the tendon and ligament experiments.

9. References

1. Kshitiz, Kim, D.-H., J., D. & Levchenko, A. Micro- and nanoengineering for stem cell biology: the promise with a caution. *Trends Biotechnol.* **29**, (2011).
2. Schenke-Layland, K. *et al.* The use of three-dimensional nanostructures to instruct cells to produce extracellular matrix for regenerative medicine strategies. *Biomaterials* **30**, 4665–75 (2009).
3. Rnjak-Kovacina, J. *et al.* Tailoring the porosity and pore size of electrospun synthetic human elastin scaffolds for dermal tissue engineering. *Biomaterials* **32**, 6729–36 (2011).
4. Yin, Z. *et al.* The regulation of tendon stem cell differentiation by the alignment of nanofibers. *Biomaterials* **31**, 2163–75 (2010).
5. Badami, A. S., Kreke, M. R., Thompson, M. S., Riffle, J. S. & Goldstein, A. S. Effect of fiber diameter on spreading, proliferation, and differentiation of osteoblastic cells on electrospun poly(lactic acid) substrates. *Biomaterials* **27**, 596–606 (2006).
6. Whited, B. M., Whitney, J. R., Hofmann, M. C., Xu, Y. & Rylander, M. N. Pre-osteoblast infiltration and differentiation in highly porous apatite-coated PLLA electrospun scaffolds. *Biomaterials* **32**, 2294–304 (2011).
7. Tucker, N., Stanger, J. J. & Staiger, M. P. The History of the Science and Technology of Electrospinning from 1600 to 1995. (1995).
8. Teo, W. E. & Ramakrishna, S. A review on electrospinning design and nanofibre assemblies. *Nanotechnology* **17**, R89–R106 (2006).
9. Ramakrishna, S., Fujihara, K., Teo, W., Lim, T.-C. & Ma, Z. *An introduction to Electrospinning and Nanofibers*. (2005).
10. Doshi, J. & Reneker, D. H. Electrospinning Process and Applications of Electrospun Fibers. *J. Electrostat.* **35**, 151–160 (1995).
11. Manee-in, J., Nithitanakul, M. & Supaphol, P. Effects of Solvent Properties , Solvent System , Electrostatic Field Strength , and Inorganic Salt Addition on Electrospun Polystyrene Fibres. **15**, 341–354 (2006).
12. Han, T., Reneker, D. H. & Yarin, A. L. Buckling of jets in electrospinning. *Polymer (Guildf)*. **48**, 6064–6076 (2007).
13. Reneker, D. H., Yarin, A. L., Fong, H. & Koombhongse, S. Bending instability of electrically charged liquid jets of polymer solutions in electrospinning. *J. Appl. Phys.* **87**, 4531 (2000).
14. Yarin, B. A. L. & Tchavdarov, B. M. Onset of folding in plane liquid films. **307**, 85–99 (1996).

15. Lyons, J., Li, C. & Ko, F. Melt-electrospinning part I : processing parameters and geometric properties. **45**, 7597–7603 (2004).
16. Jacobs, V., Anandjiwala, R. D. & Maaza, M. The Influence of Electrospinning Parameters on the Structural Morphology and Diameter of Electrospun Nanofibers. **115**, 3130–3136 (2010).
17. Beachley, V. & Wen, X. Effect of electrospinning parameters on the nano fi ber diameter and length. *Mater. Sci. Eng. C* **29**, 663–668 (2009).
18. Eichhorn, S. J. & Sampson, W. W. Statistical geometry of pores and statistics of porous nanofibrous assemblies. *J. R. Soc. Interface* **2**, 309–18 (2005).
19. Vaquette, C. & Cooper-White, J. J. Increasing electrospun scaffold pore size with tailored collectors for improved cell penetration. *Acta Biomater.* **7**, 2544–57 (2011).
20. Sun, B. *et al.* Fabrication of curled conducting polymer microfibrillar arrays via a novel electrospinning method for stretchable strain sensors. *Nanoscale* **5**, 7041–5 (2013).
21. Tang, C.-C. *et al.* Preparation of Curled Microfibers by Electrospinning with Tip Collector. *Chinese Phys. Lett.* **28**, 056801 (2011).
22. Sundaray, B. *et al.* Unusual process-induced curl and shrinkage of electrospun PVDF membranes. *Polymer (Guildf)*. **54**, 4588–4593 (2013).
23. Kessick, R. & Tepper, G. Microscale polymeric helical structures produced by electrospinning. *Appl. Phys. Lett.* **84**, 4807 (2004).
24. Trindade, A. C., Canejo, J. P., Teixeira, P. I. C., Patrício, P. & Godinho, M. H. First curl, then wrinkle. *Macromol. Rapid Commun.* **34**, 1618–22 (2013).
25. Nam, J., Huang, Y., Agarwal, S. & Lannutti, J. Improved cellular infiltration in electrospun fiber via engineered porosity. *Tissue Eng.* **13**, 2249–57 (2007).
26. Baker, B. M. *et al.* The potential to improve cell infiltration in composite fiber-aligned electrospun scaffolds by the selective removal of sacrificial fibers. *Biomaterials* **29**, 2348–58 (2008).
27. McNamara, L. E. *et al.* Nanotopographical control of stem cell differentiation. *J. Tissue Eng.* **2010**, 120623 (2010).
28. Grigoriadis, a E., Heersche, J. N. & Aubin, J. E. Differentiation of muscle, fat, cartilage, and bone from progenitor cells present in a bone-derived clonal cell population: effect of dexamethasone. *J. Cell Biol.* **106**, 2139–51 (1988).
29. Gregoire, F. M., Smas, C. M. & Sul, H. S. Understanding adipocyte differentiation. *Physiol. Rev.* **78**, 783–809 (1998).

30. Engler, A. J., Sen, S., Sweeney, H. L. & Discher, D. E. Matrix elasticity directs stem cell lineage specification. *Cell* **126**, 677–89 (2006).
31. Guvendiren, M. & Burdick, J. a. The control of stem cell morphology and differentiation by hydrogel surface wrinkles. *Biomaterials* **31**, 6511–8 (2010).
32. Kim, D.-H., Provenzano, P. P., Smith, C. L. & Levchenko, A. Matrix nanotopography as a regulator of cell function. *J. Cell Biol.* **197**, 351–60 (2012).
33. Li, W.-J., Tuli, R., Huang, X., Laquerriere, P. & Tuan, R. S. Multilineage differentiation of human mesenchymal stem cells in a three-dimensional nanofibrous scaffold. *Biomaterials* **26**, (2005).
34. Li, W.-J., Mauck, R. L., Cooper, J. A., Yuan, X. & Tuan, R. S. Engineering controllable anisotropy in electrospun biodegradable nanofibrous scaffolds for musculoskeletal tissue engineering. *Biomaterials* **40**, (2007).
35. Zhang, X., Baughman, C. B. & Kaplan, D. L. In vitro evaluation of electrospun silk fibroin scaffolds for vascular cell growth. *Biomaterials* **29**, 2217–27 (2008).
36. McBeath, R., Pirone, D. M., Nelson, C. M., Bhadriraju, K. & Chen, C. S. Cell shape, cytoskeletal tension, and RhoA regulate stem cell lineage commitment. *Dev. Cell* **6**, 483–95 (2004).
37. Born, a-K. *et al.* Correlating cell architecture with osteogenesis: first steps towards live single cell monitoring. *Eur. Cell. Mater.* **18**, 49–60, 61–2; discussion 60 (2009).
38. Gao, L., McBeath, R. & Chen, C. S. Stem cell shape regulates a chondrogenic versus myogenic fate through Rac1 and N-cadherin. *Stem Cells* **28**, 564–72 (2010).
39. Cell, S. & Properties, M. Cytoskeletal and Focal Adhesion Influences. **18**, 436–444 (2012).
40. Yu, H. *et al.* Insights into the role of focal adhesion modulation in myogenic differentiation of human mesenchymal stem cells. *Stem Cells Dev.* **22**, 136–47 (2013).
41. Lui, P. P. Y., Rui, Y. F., Ni, M. & Chan, K. M. Tenogenic differentiation of stem cells for tendon repair - what is the current evidence? *J. Tissue Eng. Regen. Med.* (2011).
42. Liu, Y., Ramanath, H. S. & Wang, D.-A. Tendon tissue engineering using scaffold enhancing strategies. *Trends Biotechnol.* **26**, 201–9 (2008).
43. Shearn, J. T. *et al.* Tendon tissue engineering: progress, challenges, and translation to the clinic. *J. Musculoskelet. Neuronal Interact.* **11**, 163–73 (2011).
44. Smith, L. *et al.* Tissue engineering strategies for the Tendon/ligament-to-bone insertion. **53**, 95–105 (2013).

45. Wang, J. H. C. Mechanobiology of tendon. *J. Biomech.* **39**, (2006).
46. Hulmes, D. J. S. Building Collagen Molecules, Fibrils, and Suprafibrillar Structures. *J. Struct. Biol.* **137**, 2–10 (2002).
47. Silver, F., Freeman, J. & Seehra, G. Collagen self-assembly and the development of tendon mechanical properties. *J. Biomech* **10**, (2003).
48. Tong, W. Y. *et al.* Functional replication of the tendon tissue microenvironment by a bioimprinted substrate and the support of tenocytic differentiation of mesenchymal stem cells. *Biomaterials* **33**, 7686–98 (2012).
49. Li, W.-J., Danielson, K. G., Alexander, P. G. & Tuan, R. S. Biological response of chondrocytes cultured in three-dimensional nanofibrous poly(epsilon-caprolactone) scaffolds. *J. Biomed. Mater. Res. A* **67**, 1105–14 (2003).
50. Spalazzi, J. P., Vyner, M. C., Jacobs, M. T., Moffat, K. L. & Lu, H. H. Mechanoactive scaffold induces tendon remodeling and expression of fibrocartilage markers. *Clin. Orthop. Relat. Res.* **466**, 1938–48 (2008).
51. Aou, K., Kang, S. & Hsu, S. L. Morphological Study on Thermal Shrinkage and Dimensional Stability Associated with Oriented Poly(lactic acid). *Macromolecules* **38**, 7730–7735 (2005).
52. Abe, M. *et al.* An assay for Transforming Growth Factor-B using cells transfected with a Plasminogen Activator Inhibitor-1 Promoter-Luciferase construct. *Anal. Biochem.* 274–284 (1994).
53. Baker, B. M. *et al.* The potential to improve cell infiltration in composite fiber-aligned electrospun scaffolds by the selective removal of sacrificial fibers. *Biomaterials* **29**, 2348–2358 (2008).
54. Wójciak, B., Crossan, J., Curtis, A. S. G. & Wilkinson, C. D. W. Grooved substrata facilitate in vitro healing of completely divided flexor tendons. *J. Mater. Sci. Mater. Med.* **6**, 266–271 (1995).
55. Raspanti, M., Alessandro, M., Franchib, M. & Ruggerib, A. The 3D structure of crimps in the rat Achilles tendon. *Matrix Biol.* **24**, 503–507 (2005).
56. Yasuda, K., Tomita, F., Yamazaki, S., Minami, A. & Tohyama, H. The effect of growth factors on biomechanical properties of the bone-patellar tendon-bone graft after anterior cruciate ligament reconstruction: a canine model study. *Am. J. Sports Med.* **32**, (2004).
57. Alan, D. F. & Todd, C. D. Elastic Model for Crimped Collagen Fibrils. *J. Biomed. Eng.* **127**, (2005).